NATIONAL ADVISORY COMMITTEE FOR AERONAUTICS

TECHNICAL MEMORANDUM 1351

ON THE DESIGN OF AIRFOILS IN WHICH THE TRANSITION OF THE BOUNDARY LAYER IS DELAYED

By Itiro Tani

Translation of "Kyōkaiso no Sen'i o okuraseru Yokugata ni tuite." Report of the Aeronautical Research Institute, Tokyo Imperial University, No. 250 (vol. 19, no. 1), Jan. 1943

Washington
October 1952

1R

NATIONAL ADVISORY COMMITTEE FOR AERONAUTICS

TECHNICAL MEMORANDUM 1351

ON THE DESIGN OF AIRFOILS IN WHICH THE TRANSITION OF THE BOUNDARY LAYER IS DELAYED*

By Itiro Tani

INTRODUCTION - LAMINAR-FLOW AIRFOILS

1. In high speed flight conditions, the drag of an airfoil is almost exclusively due to skin friction. Therefore, if further reduction in drag is desired, it is necessary to delay as much as possible the transition from laminar to turbulent flow in the boundary layer along the surface, thus decreasing the extent of the turbulent boundary layer which gives considerable skin friction. As the factors that may affect the transition, we will consider the stream turbulence, the surface roughness, the surface pressure distribution, and so on. In actual flight conditions, however, the effect of turbulence seems to be unexpectedly small, so that, so far as smooth surfaces are concerned, there remains only the shape of the airfoil section in relation to pressure distribution as the most important factor affecting transition. We call a laminar-flow airfoil that airfoil in which the shape of the section is suitably designed so as to delay the transition of the boundary layer flow.

2. It is evident that the laminar separation of the boundary layer may cause the transition, as will be mentioned in the appendant part of the paper, paragraphs 35-40. We cannot expect, therefore, to maintain laminar flow beyond the separation point. Summarizing the results of flight experiments on airfoils hitherto made (refs. 8 to 12), we have the conclusion that the observed transition coincides approximately with the calculated laminar separation point at small Reynolds numbers, while it moves upstream toward the minimum pressure point as the Reynolds number increases. However, no example has ever yet been observed in which the transition moves ahead of the minimum pressure point. We therefore arrive at the supposition that the laminar-flow airfoil may be most simply realized by designing the airfoil in which the minimum pressure occurs well downstream.

---

*"Kyōkaiso no Sen'i o okuraseru Yokugata ni tuite." Report of the Aeronautical Research Institute, Tokyo Imperial University, No. 250 (vol. 19, no. 1), Jan. 1943.

DESIGN OF SYMMETRICAL AIRFOILS IN WHICH THE MINIMUM PRESSURE OCCURS DOWNSTREAM

3. Following Professor Moriya (ref. 13), we write the coordinate along the chord in the form $x = \frac{1}{2}(1 + \cos \xi)$, and assign $x = 0$, $\xi = \pi$ to the leading edge, and $x = 1$, $\xi = 0$ to the trailing edge. Expressing the ordinate of the mean camber line by $M = \sum_0^\infty a_n \cos n\xi$, and the half-thickness measured normal to the chord by $T = \sum_1^\infty b_n \sin n\xi$ [1], the pressure distribution around the airfoil in the two-dimensional potential flow is given by

$$\frac{p}{q} = 1 - \frac{\left[\cos\alpha\left\{\mp\frac{1}{2}\sin\xi + \sum_1^\infty na_n(1-\cos n\xi) \mp \sum_1^\infty nb_n \sin n\xi\right\} + \sin\alpha\left\{-\frac{1}{2}(1-\cos\xi) \mp \sum_1^\infty na_n \sin n\xi + \sum_1^\infty nb_n \cos n\xi\right\}\right]^2}{\frac{1}{4}\sin^2\xi + \left\{\mp\sum_1^\infty na_n \sin n\xi + \sum_1^\infty nb_n \cos n\xi\right\}^2}$$

$$= 1 - \frac{\left[\cos\alpha\left\{1 \pm fA_c + eB_s\right\} + \sin\alpha\left\{\pm\sqrt{\frac{1-x}{x}} - \left(fA_s \pm eB_c\right)\right\}\right]^2}{1 + \left(fA_s \pm eB_c\right)^2}$$

[1] The ordinates of the upper and lower surfaces are given by $M + T$ and $M - T$, respectively.

where α is the angle of attack, p is the pressure acting on the airfoil surface, measured from the static pressure of the undisturbed stream, and q is the dynamic pressure of the undisturbed stream. We assume that the trailing edge is sharp, so that $\sum_1^\infty nb_n = 0$. We limit the range of the variables ξ between 0 and π, and assign the upper and lower parts of the double sign for the upper and lower surfaces, respectively. Writing f for the maximum value of M (the maximum camber) and e for the maximum value of $2T$ (the maximum thickness), we put

$$fA_c = -2\sum_1^\infty na_n \frac{1 - \cos n\xi}{\sin \xi} \qquad fA_s = -2\sum_1^\infty na_n \frac{\sin n\xi}{\sin \xi} = -\frac{dM}{dx}$$

$$eB_s = 2\sum_1^\infty nb_n \frac{\sin n\xi}{\sin \xi} \qquad eB_c = 2\sum_1^\infty nb_n \frac{\cos n\xi}{\sin \xi} = -\frac{dT}{dx}$$

The lift coefficient is given by

$$C_L = 2\pi\left\{\sin \alpha - 2\sum_1^\infty na_n \cos \alpha\right\}$$

We consider first only the thickness of the airfoil (the camber of the center line will be considered in the next section, paragraphs 8 to 11). Namely, we consider the symmetrical airfoil section set at zero angle of attack, with a view to obtaining the minimum pressure well downstream.

4. We adopt as the typical example of the commonly used symmetrical airfoils the NACA symmetrical airfoil (ref. 14)

$$T = e\left\{1.4845\sqrt{x} - 0.6300x - 1.7580x^2 + 1.4215x^3 - 0.5075x^4\right\}$$

The maximum thickness is located at $x = 0.3$, the leading-edge radius is $1.1e^2$, and the trailing-edge slope $-(dT/dx)_{x=1}$ is $1.17e$. The pressure distribution for the case $e = 0.1$ is shown in figure 1. The minimum pressure is located at $x = 0.1$, and the laminar separation point, determined by the approximate method due to the author (refs. 15 and 16),

at $x = 0.61$. If the transition point of the boundary layer would not move upstream beyond the laminar separation point, we might expect to maintain a laminar boundary layer for more than half the surface of the airfoil. The flight experiments hitherto made, however, appear to give negative evidence for such a conjecture.

5. Now, in order to shift the minimum pressure backward, it is required to shift the position of maximum thickness ($x = m$) backward. For designing such airfoils, we represent the shapes of parts before and after the maximum thickness by two algebraic expressions. For the forward half ($0 \leqq x \leqq m$)

$$T = e\left\{\sqrt{2hx} + h_1 x + h_2 x^2\right\}$$

while for the rear half ($m \leqq x \leqq 1$)

$$T = e\left\{0.01 + d_1(1 - x) + d_2(1 - x)^2 + d_3(1 - x)^3\right\}$$

where

$$h_1 = \frac{2 - 3\sqrt{2hm}}{2m} \qquad h_2 = \frac{\sqrt{2hm} - 1}{2m^2}$$

$$d_2 = \frac{1.47 - 2d_1(1 - m)}{(1 - m)^2} \qquad d_3 = \frac{d_1(1 - m) - 0.98}{(1 - m)^3}$$

and we assign arbitrary values for three parameters, m, h (= leading-edge radius $\doteqdot e^2$), and d_1 (= trailing-edge slope $\doteqdot e$). Although the method has the drawback that the two expressions give different values of d^2T/dx^2 at $x = m$, where dT/dx becomes zero, we nevertheless adopt it because we are in a position to vary the forward and rearward parts most simply and independently.

6. First, we fix the forward half with $m = 0.5$ and $h = 0.5$, and vary the rear half by giving d_1 the values 1.7, 2.0, 2.5, and 3.0, respectively. The shape of the section and the pressure distribution for $e = 0.1$ are shown in figure 2. We find from this result that, as

d_1 increases, the minimum pressure point moves backward and the gradient of pressure rise following the minimum pressure steepens. We also find that the pressure distribution in the neighborhood of the minimum pressure exhibits a wavy indentation when the value of d_1 is too small or too large, and that there exists a certain value of d_1 for which the pressure distribution is flat and smooth. Such a value of d_1 is about 2.5 in this case. We therefore fix the rear half with $d_1 = 2.5$, and vary the forward half by giving h the values 0.35, 0.50, 0.70, and 1.05, respectively. The shape of the section and the pressure distribution for $e = 0.1$ are shown in figure 3. From this comparison, we find that the negative pressure bump immediately behind the leading edge decreases as h decreases, and that the maximum permissible value of h is about 0.7.

The effect of thickness is shown in figure 4, in which curves of pressure distribution are given for different values of e, 0.06, 0.10, and 0.14, but for a fixed set of parameters, $m = 0.5$, $h = 0.5$, and $d_1 = 2.5$. It is seen that the characteristics of the pressure distribution do not materially change with thickness. There is, however, a slight change in the pressure distribution, the maximum permissible value for h slightly increasing as the thickness increases.

To see the effect of the position of maximum thickness, we give m values ranging from 0.35 to 0.60, varying at the same time values of d_1 and h so that the pressure distribution becomes flat and smooth. The result of calculation is given in figure 5, which shows a considerable change in the position of minimum pressure. The change is not purely due to the effect of m, but it is at any rate to be noticed that the value of m less than 0.4 is not sufficient for shifting backward the minimum pressure, while increasing the value of m beyond 0.5 is of no advantage, since the backward shift is then almost saturated, only the adverse pressure gradient being increased.

7. From the results of calculation, we thus arrive at the conclusion that m must be between 0.4 and 0.5 and h must be less than 0.7 in order that the minimum pressure occurs well downstream. Smaller values of h are desirable, but, on the other hand, we should like to make h as large as possible, because a large value of h will be advantageous in increasing the maximum lift coefficient and in preventing the inception of adverse pressure gradient when the angle of attack is slightly changed. Even if we give h the maximum permissible value 0.7, the leading-edge radius amounts to only 60 percent of that for the conventional NACA symmetrical airfoil of the same thickness. In order to increase the leading-edge radius, it is required to increase the thickness, which in turn is accompanied by an increase in adverse pressure gradient following the minimum pressure. The adverse pressure gradient should be kept within a

certain limit, so that it becomes necessary to make a compromise between conflicting requirements. Thus, we are no longer in a position to require the farthest possible rearward location of the minimum pressure. We should also use a value of d_1 which is somewhat smaller than that mentioned previously.

Taking these requirements into account, we finally arrive at the design of a series of symmetrical airfoil sections, the parameters of which are given in the following table:

Section	m	h	d_1	Position of minimum pressure
I	0.500	0.35	2.384	0.63
J	.500	.54	1.800	.55
K	.475	.56	1.575	.51
L	.450	.58	1.400	.47
M	.400	.62	1.150	.37
N	.350	.66	1.000	.24

Although section I is the most ideal for delaying the transition, in practice, its extraordinarily sharp nose and blunt tail are drawbacks. On the other hand, section N is too much compromised. Sections K or L seem to be suitable as laminar-flow airfoils for practical use. The ordinates of these six sections are given in table 1, while the auxiliary functions B_s and B_c associated with the pressure distribution (see paragraph 3) are given in tables 2 and 3, respectively. The shapes of the airfoil sections and the pressure distribution for $e = 0.1$ are shown in figure 6.

DESIGN OF MEAN CAMBER LINE SUITABLE FOR LAMINAR-FLOW AIRFOILS

8. A symmetrical airfoil set at zero angle of attack has no lift. In order to obtain lift, the center line of the symmetrical airfoil must be curved with a suitable camber. Since the effects of thickness and camber are nearly additive with regard to the pressure distribution, the mean camber line which maintains the nature of the pressure distribution of the symmetrical airfoil will be such that it shall give a uniform distribution of pressure difference when the thickness is removed. Evidently, the center of pressure is then located at $x = 0.5$, so that such a camber line has the drawback that the travel of center of pressure is considerable. To reduce the travel of center of pressure, the uniformity of pressure difference should be satisfied only in the forward part of the chord. From the standpoint of designing the laminar-flow airfoil, however, it is

only required that the distribution of pressure difference is uniform from the leading edge to that point corresponding to the minimum pressure of the symmetrical airfoil.

9. When the angle of attack α is small, the expression for pressure distribution given in paragraph 3 may be put into the form

$$\frac{p}{q} = 1 - \frac{\left[\left(1 + eB_s\right) \pm \left(fA_c + \sqrt{\frac{1-x}{x}}\,\alpha\right) - \left(fA_s \pm eB_c\right)\alpha\right]^2}{1 + \left(fA_s \pm eB_c\right)^2}$$

Since the effect of the term $\left(fA_s \pm eB_c\right)$ is very small, the quantity

$$fG \equiv fA_c + \sqrt{\frac{1-x}{x}}\,\alpha$$

is required to be constant in order that the camber line shall not change the nature of the pressure distribution of the symmetrical section. The range of constancy is at least up to the position of minimum pressure of the symmetrical section. Putting $\cos \xi = u = 2x - 1$, and considering for simplicity the case when the minimum pressure is located at $u = 0$, we prescribe that

$G = \text{constant} = G_0$ for $0 \leqq x \leqq 0.5$, $-1 \leqq u \leqq 0$

$G = G_0(1 - u^2)^m$, $m \geqq 0$ for $0.5 \leqq x \leqq 1$, $0 \leqq u \leqq 1$

See figure 7. Moreover, since

$$fG = -2\sum_{1}^{\infty} na_n \frac{1 - \cos n\xi}{\sin \xi} + \frac{1 - \cos \xi}{\sin \xi}\,\alpha$$

α cannot be arbitrary, but must be so chosen that the right side of the equation does not become infinite at the leading edge, $\xi = \pi$. It is given by

$$\alpha = 2 \sum_{1}^{\infty}{}' n a_n$$

where $(')$ denotes that only odd integers should be taken for n. This is the so-called ideal angle of attack due to Theodorsen (ref. 17). Using the assumption of the thin wing theory, we neglect the terms eB_s and $\left(fA_s \pm eB_c\right)$. We then have

$$C_L = 2\left(1 + \sigma_m\right) f G_0 \qquad \sigma_m = \int_0^{\pi/2} \sin^{2m+1}\xi \, d\xi$$

$$C_{m0} = - \frac{1 + (1 + m)\sigma_m}{4(1 + m)(1 + \sigma_m)} C_L$$

$$\alpha = 2 \sum_{1}^{\infty} n a_n + \frac{C_L}{2\pi}$$

where C_{m0} is the moment coefficient about the leading edge (positive when nose up) at $C_L = 0$. Although $m = 0$ corresponds to the case of making G uniform up to the trailing edge, it seems to be impossible to realize a finite pressure difference at the trailing edge. Moreover, the quantity $-C_{m0}/C_L$ (which represents the degree of center of pressure travel) is as large as 0.25 in this case. If $m > 0$, G vanishes at the trailing edge, and $-C_{m0}/C_L$ decreases as m increases, tending to 0 as m approaches ∞. $m = \infty$ corresponds to the case when $G = 0$ in the rear half of the chord. Increasing the value of m, however, steepens the pressure gradient, so the value of m from 3 to 5 seems to be adequate.

Now, since

$$fG \sin \xi = 2 \sum_1^\infty na_n \cos n\xi - \left(2 \sum_1^\infty na_n + \frac{C_L}{2\pi} \right) \cos \xi + \frac{C_L}{2\pi}$$

the slope of the camber line having the prescribed distribution of G is given by

$$\frac{dM}{dx} = 2 \sum_1^\infty na_n \frac{\sin n\xi}{\sin \xi} = -\frac{1}{\pi} \int_0^\pi 2 \sum_1^\infty na_n \cos n\xi' \frac{d\xi'}{\cos \xi - \cos \xi'}$$

$$= \frac{C_L}{2\pi} \left[1 + \frac{1}{1 + \sigma_m} \left\{ \log \frac{u}{1 + u} + (1 - u^2)^m \log \frac{1 - u}{u} + \int_0^1 \frac{(1 - u^2)^m - (1 - v^2)^m}{u - v} dv \right\} \right] + 2 \sum_1^\infty na_n$$

The ordinate of the camber line is obtained by the integration

$$M = \int_0^x \frac{dM}{dx} dx$$

$\sum_1^\infty na_n$ may be determined by the condition that $M = 0$ at $x = 1$. We call D_m the camber line thus determined. The equations for camber lines for $m = 0, 1, 3, 5,$ and ∞, namely D_0, D_1, D_3, D_5, and D_∞,

are given below, their important characteristics being summarized in the table. It is to be noted that f is the maximum value of M, ϵ is the absolute value of the zero-lift angle, and ϵ and α are measured in radians.

m	α/C_L	ϵ/C_L	f/C_L	$-C_{m0}/C_L$
0	0	0.1592	0.0552	0.2500
1	.0380	.1211	.0711	.1750
3	.0609	.0983	.0790	.1213
5	.0703	.0888	.0816	.0979
∞	.1103	.0488	.0874	0

$$D_0: \quad \frac{M}{f} = 1 - \frac{1}{2 \log 2}\left\{(1 - u) \log (1 - u) + (1 + u) \log (1 + u)\right\}$$

$$D_1: \quad \frac{4\pi}{C_L} M = \frac{1}{5}(5 + u) \log 2 - \frac{3}{5}(1 + u) \log (1 + u) + \frac{1}{5} u^3 \log |u| -$$

$$\frac{1}{5}(1 - u)^2(2 + u) \log (1 - u) + \frac{1}{5}(1 - u^2)$$

$$D_3: \quad \frac{4\pi}{C_L} M = \frac{1}{51}(51 + 19u) \log 2 - \frac{35}{51}(1 + u) \log (1 + u) +$$

$$\frac{1}{51} u^3\left(35 - 21u^2 + 5u^4\right) \log |u| -$$

$$\frac{1}{51}(1 - u)^4(16 + 29u + 20u^2 + 5u^3) \log (1 - u) +$$

$$\frac{1}{612}(1 - u^2)(176 - 81u - 172u^2 + 30u^3 + 60u^4)$$

$$D_5: \quad \frac{4\pi}{C_L} M = \frac{1}{949}(949 + 437u) \log 2 - \frac{693}{949}(1 + u) \log (1 + u) +$$

$$\frac{1}{949} u^3 \left(1155 - 1386u^2 + 990u^4 - 385u^6 + 63u^8\right) \log |u| -$$

$$\frac{1}{949} (1 - u)^6 \left(256 + 843u + 1218u^2 + 938u^3 + 378u^4 +\right.$$

$$\left. 63u^5\right) \log (1 - u) + \frac{1}{113880} (1 - u^2) \left(35072 - 28535u - 66088u^2 +\right.$$

$$\left. 31680u^3 + 68792u^4 - 17430u^5 - 36120u^6 + 3780u^7 + 7560u^8\right)$$

$$D_\infty: \quad \frac{M}{f} = \frac{1}{\log 3} \left\{(1 + u) \log 2 - (1 + u) \log (1 + u) + u \log |u|\right\}$$

Shapes of these camber lines are shown in figure 7, the ordinates of them are given in table 4, and the auxiliary functions A_c and A_s (see paragraph 3) and the pressure difference distribution G are given in tables 5, 6, and 7, respectively.

10. The calculation made previously is only approximate, neglecting the thickness. It is therefore desirable to check the result by actually calculating the pressure distribution for the specified angle of attack taking both camber and thickness into account. As an example, we construct an airfoil by applying the thickness form K with $e = 0.15$ normal to the chord around the camber line D_5 with $f = 0.02$ (the resulting airfoil is designated as $D_5K - 2015$). We calculate the pressure distribution by the formula of paragraph 3 for the optimum design condition $\alpha = 0.99^\circ$ and $C_L = 0.245$. The result is shown in figure 8. The nature of the pressure distribution remains similar to that of the symmetrical airfoil, so we may consider that the approximate determination neglecting thickness gives results sufficiently accurate for practical purposes.

11. In designing the camber line D_m, we have assumed for simplicity that the pressure difference G is constant for $u \leqq 0$. This corresponds to the case when the symmetrical airfoil has its minimum pressure in the

neighborhood of $u = 0$. Therefore, the camber line D_m is adequate to be combined with the symmetrical section J or K. If, however, the symmetrical section is adopted in which the minimum pressure is located further upstream, it is not only not neoessary to maintain G constant up to $u = 0$, but also of disadvantage because it makes it difficult to reduce the value of $-C_{m0}/C_L$.

To reduce the range over which G should be maintained constant, we may proceed in the following way. Assuming for instance that G should be constant from $u = -1$ to $u = -\frac{1}{3}$, and using a new variable $u_1 = \frac{1}{4}(1 + 3u)$, we prescribe that

$$G = G_0 \qquad \text{for} \quad -1 \leqq u \leqq -\frac{1}{3}, \quad -\frac{1}{2} \leqq u_1 \leqq 0$$

$$G = G_0(1 - u_1^2)^3 \qquad \text{for} \quad -\frac{1}{3} \leqq u \leqq 1, \quad 0 \leqq u_1 \leqq 1$$

The calculation may be performed similarly to the case of D_m. The resulting camber line is designated as F_3. The camber line lying in the middle between F_3 and D_5 is also designed, and designated as E_4. Their important characteristics are given in the following table together with those of D_5. Other numerical data for these camber lines are given in tables 4 to 7.

Camber line	α/C_L	ϵ/C_L	f/C_L	$-C_{m0}/C_L$
D_5	0.0703	0.0888	0.0816	0.0979
E_4	.0752	.0840	.0813	.0859
F_3	.0764	.0827	.0795	.0833

Since the camber lines E_4 and F_3 enable us to maintain G constant up to the point $x = 0.42$ and $x = 0.33$, respectively, they are adequate to be combined with the symmetrical sections L and M, respectively. The pressure distribution is shown in figure 10 for the airfoil obtained by applying the thickness form M with $e = 0.15$ around the camber line F_3 with $f = 0.02$. The optimum design condition corresponds to $\alpha = 1.10^\circ$ and $C_L = 0.252$.

EXPERIMENTS ON LAMINAR-FLOW AIRFOILS

12. In order to ascertain whether it is possible to prevent the forward movement of the boundary layer transition by shifting the minimum pressure on the airfoil surface, we have to perform experiments in a low turbulence wind tunnel or on the actual airplane in flight. When the Reynolds number is not too large, however, we can still use a conventional wind tunnel in which the stream turbulence is relatively small. So we made at first comparative measurements on two symmetrical airfoils, NACA 0010 and L.B. 24 in the 1.5 m wind tunnel of the Aeronautical Research Institute. L.B. 24 is a laminar-flow airfoil of 10 percent thickness, already shown in figure 3. The theoretical pressure distribution is also given in figure 11. The minimum pressure is located at $x = 0.64$, and the laminar separation at $x = 0.77$. The wind tunnel was of the lowest turbulence level available for the author, the critical Reynolds number of a sphere being 3.66×10^5 and the transition Reynolds number of a flat plate 1.05×10^3 (see paragraph 28). In order to raise the Reynolds number as high as possible, unusually large models were used. They were made of laminated mahogany, of highly polished surface, of 0.8 m span, of 1.2 m chord, and fitted with end plates 1.3 m × 0.6 m. Since the model was large compared with the size of the tunnel and the end plates were not sufficiently large, the results for a given airfoil may not correspond even approximately with those for the same airfoil in an undisturbed two-dimensional flow. Our object, however, was merely to ascertain the relation between pressure distribution and transition, and it seemed reasonable to expect that the relation will not be seriously affected by limitations in the conditions of the experiments. As a matter of fact, marked difference was found in the calculated and measured distributions of pressure, the latter of which was measured along the median section of the model with a static tube of 1 mm diameter (fig. 12).[2] This discrepancy, however, is immaterial, since our object was merely to compare the two airfoils, both of which are affected quite similarly by experimental limitations.

13. The angle of attack of the model was zero, and the wind speed was varied from 6 to 40 m/s. The local drag of the median section was determined from wake measurements, that were made in the section 11 cm behind the trailing edge. Measurements of static and total pressures in the wake were made, respectively, with a static tube of 2.5 mm external diameter and a pitot tube with a flattened mouth of 0.65 mm external depth and 2.6 mm width. The profile drag coefficient C_{D_0} was obtained

---

[2]The measured values are those for a Reynolds number of about 2×10^6. The distribution of pressure changes but little with the Reynolds number.

from the measured pressures by Jones' formula (ref. 18). Figure 13 [3] presents C_{D_0} plotted against Reynolds number R referred to chord length. For a lower range of R, the drag of L.B. 24 is higher than that of NACA 0010, the reason probably being that a turbulent boundary layer associated with the laminar separation is established at a higher Reynolds number for the former airfoil than for the latter. For a higher range of R, however, the condition is reversed, L.B. 24 giving a drag less than half that of NACA 0010 for R higher than 2×10^6. This is probably due to the fact that the transition may occur much later for L.B. 24 than it does for NACA 0010, as also observed from the comparison of wake conditions for the two airfoils (fig. 14).[4]

14. In order to verify the aforementioned supposition, a pitot tube with a flattened mouth of external depth 0.9 mm and width 2.7 mm was placed in contact with the airfoil surface, and the wind speed, and consequently the Reynolds number R, were determined at which the indicated total pressure G* divided by the dynamical pressure q of the undisturbed stream begins to rise suddenly. The results are shown in figure 15. From this figure, the dependence of the transition point on Reynolds number as shown in figure 16 is obtained. At the same Reynolds number, the transition occurs much farther from the leading edge for L.B. 24 than for NACA 0010. Even at the highest Reynolds number reached, L.B. 24 has a transition as far back as $x = 0.80$. This is somewhat beyond the laminar separation point, $x = 0.77$, which is calculated from the theoretical pressure distribution. However, this is not contradictory, because the actual pressure distribution differs from the theoretical one in a manner to delay the transition (fig. 12).

15. With further increase in Reynolds number, the transition may move toward the leading edge, but it seems improbable that the transition moves forward beyond the minimum pressure. It is highly desirable to check this point also by wind tunnel experiments, but all the wind tunnels now available to the author are of no use for making measurements at sufficiently high Reynolds numbers, because the transition is prematurely

---

[3] In this figure, the curves L and T represent the drag of a flat plate when the boundary layer is entirely laminar and entirely turbulent, respectively. The curves NV and NF represent the drag of airfoil NACA 0009 measured in the NACA Variable-Density Wind Tunnel and NACA Full-Scale Wind Tunnel, respectively.

[4] In this figure G and p are the total and static pressures in the wake, respectively, and G_0 is the total pressure outside the wake, all being measured from the static pressure of the undisturbed stream. y is the distance across the wake, and t is the chord of the model.

induced by the turbulence of the stream (see paragraphs 27 to 29). It seems urgent to build a special wind tunnel of low turbulence level. For the present, however, it is simplest to rely upon experiments in actual flight. Such a hope of the author was fortunately realized by the specially planned flight experiment, which was performed at the Navy Aeronautical Technical Arsenal (ref. 19).

16. The airplane used for the experiment was a biplane; two portions of the lower wing, each of 1.1 m span, were covered with the airfoil to be tested. The test portions were of chord 2.4 m, made of Japanese Hinoki, highly polished, and fitted with a partition fence of small height at both ends. Two test portions were placed symmetrically, pressure distribution and wake measurements being performed on the starboard portion, while the boundary layer was observed on the port portion. The airfoil section was not one of the most appropriate design now considered, because it was required to put it on the original section of the airplane, and, moreover, to determine the section before completion of the final design calculation. It has the following characteristics:

Mean camber line: $M = 0.0667x(1 - x)(1 - x + x^2)$, $f = 0.0125$

Thickness distribution: $e = 0.12$, $m = 0.45$, $h = 0.56$, $d_1 = 1.60$

The camber line is similar to D_0 of paragraph 9, but there exists a slight lack of uniformity of G in the neighborhood of leading and trailing edges. The thickness distribution is similar to L of paragraph 7, but the trailing edge slope is somewhat larger than L.

17. Results of flight experiments are summarized in figure 17 and 18. In figure 17, the section lift coefficient C_L, obtained by integrating the pressure distribution curve, is shown by a broken line plotted against the Reynolds number R referred to the flight speed and chord length, and C_L is again shown by a solid line plotted against the profile drag coefficient C_{D_0} determined from the wake measurements. In figure 18, the measured pressure distribution is shown in comparison with the theoretical one (two-dimensional potential flow) having the same value of C_L. The transition points estimated from the change in boundary layer velocity profiles are also marked. Generally speaking, the measured pressure distribution agrees fairly well with the theoretical one, although a slight difference appears when C_L becomes large. An adverse pressure gradient is found on the lower surface when C_L is small, thus resulting in the transition point being observed unexpectedly far forward. Such a discrepancy in pressure distribution as compared with the theoretical one seems to be probably due to the fact that the span of the test portion was not sufficiently large. As a result, the profile drag coefficient C_{D_0} has the minimum value 0.0042

at about $C_L = 0.26$, which is larger than the value $C_L = 0.18$ theoretically estimated on the assumption that the transition occurs far back on both upper and lower surfaces. Therefore, the observed value of C_{D_0}, although much smaller than that of the conventional airfoils, seems to be still somewhat large when compared with the optimum case. At any rate, however, no transition was found to occur upstream of the minimum pressure. It is important to note that such experimental evidence was obtained on an airfoil section in which the minimum pressure is located further downstream than on the conventional one. This finding will give valuable data to establish a basis for design of the laminar-flow airfoils.

ESTIMATION OF THE DRAG OF LAMINAR-FLOW AIRFOILS

18. As mentioned previously, the results of flight experiments seem to support the basis for the design of laminar-flow airfoils, namely, the possibility of maintaining the boundary layer laminar at least up to the minimum pressure point. It is interesting, therefore, to estimate the drag of laminar-flow airfoils by assuming a laminar boundary layer from the leading edge to the minimum pressure point and a turbulent boundary layer downstream to the trailing edge.

For the laminar boundary layer, the momentum thickness is given by

$$\theta^2 = \frac{0.44\nu}{u_1^5} \int_0^s u_1^4 \, ds$$

with a sufficient approximation (ref. 16), where u_1 is the velocity outside the boundary layer and s is the distance measured along the airfoil surface from the forward stagnation point. Writing t for the chord length and V for the velocity of the undisturbed flow (velocity of flight), and putting

$$u_1 = UV \qquad s = \sigma t \qquad R = \frac{Vt}{\nu}$$

we have the nondimensional expression

$$\frac{\theta_a^2}{t^2} = \frac{0.44}{RU_a}\int_0^{\sigma_a}\left(\frac{U}{U_a}\right)^4 d\sigma$$

where the subscript a refers to the point of minimum pressure. Applying then the solution due to Buri (ref. 20) for a turbulent boundary layer assumed to extend from the minimum pressure point to the trailing edge, we have the result

$$\left[\left(\frac{\theta}{t}\right)^{5/4}U^{17/4}\right]_{\sigma_a}^{\sigma_b} = 0.0162R^{-1/4}\int_{\sigma_a}^{\sigma_b} U^4\, d\sigma$$

where the subscript b refers to the trailing edge. The numerical values originally given by Buri are slightly modified so as to agree with measurements when applied to the flat plate.

According to Squire and Young (ref. 21), the profile drag coefficient is given by

$$C_{D_0} = \frac{2}{t}\left(\theta_u + \theta_l\right)_b U_b^{3.2}$$

where the subscripts u and l refer to the upper and lower surfaces, respectively. The exponent 3.2 of U_b has been obtained by assuming the ratio of displacement and momentum thicknesses equal to 1.4. But the ratio seems to exceed 1.4 near the trailing edge, so we replace 3.2 by 3.4 with a view to improving the accuracy and at the same time to simplifying the algebra. Since

$$\frac{\theta_b}{t}U_b^{3.4} = \left[\left(\frac{\theta_a}{t}\right)^{5/4}U_a^{17/4} + 0.0162R^{-1/4}\int_{\sigma_a}^{\sigma_b} U^4\, d\sigma\right]^{4/5}$$

we have

$$C_{D_0} = 0.074R^{-1/5}\left[\left(L_u R^{-3/8} + T_u\right)^{4/5} + \left(L_l R^{-3/8} + T_l\right)^{4/5}\right]$$

where

$$L = 37U_a^{9/8}\left[\int_0^{\sigma_a} U^4\, d\sigma\right]^{5/8} \qquad T = \int_{\sigma_a}^{\sigma_b} U^4\, d\sigma$$

If the velocity distribution $u_l = UV$ is calculated by assuming the potential flow of an ideal fluid, it is desirable to modify the distribution to take account of the effect of separation near the trailing edge. We tentatively modified the distribution of U such that the Buri parameter $\Gamma = \left(\theta/u_l\right)\left(du_l/ds\right)\left(u_l\theta/\nu\right)^{1/4}$ at the trailing edge for the case when the boundary layer is assumed turbulent from the leading edge, namely

$$\Gamma = \frac{0.0081}{U_b^6}\left(\frac{dU^2}{d\sigma}\right)_b \int_0^{\sigma_b} U^4\, d\sigma$$

shall not become smaller than -0.06. In almost all the cases, values of U_b thus modified are found in the range between 0.95 and 1.00.

19. Applying this method of calculation, the profile drag coefficient C_{D_0} is estimated first for a series of symmetrical airfoils set at zero angle of attack. The series consists of the six symmetrical airfoils, I, J, K, L, M, N, as given in paragraph 7 and the NACA conventional airfoil. Values of C_{D_0} at $R = 2 \times 10^7$ for three different thicknesses (maximum thickness in terms of chord $e = 0.10, 0.15, 0.20$) are shown in figure 19 plotted against the position of minimum pressure. C_{D_0} seems to decrease almost linearly as the minimum pressure is shifted backward, the most ideal airfoil I giving a value about half of that of the NACA conventional airfoil. If it is desired to realize a profile drag of two-thirds of the conventional airfoil, it will be required to use the symmetrical airfoil L with the maximum thickness located at 45 percent chord from the leading edge.

Effect of camber is relatively small. If, for instance, the center line of the symmetrical airfoil K with $e = 0.15$ is curved into the camber line D_5 with $f = 0.02$ (see paragraph 9), the estimated increase in profile drag at the optimum angle of attack is only 0.0001. For $f = 0.04$, it is 0.0003.

Finally, we compare the laminar-flow airfoil with the most extensively used airfoil, NACA 23012, for which the leading-edge radius is 0.0158, and the optimum lift coefficient corresponding to the minimum profile drag coefficient is about 0.15. If we consider the symmetrical airfoil section K ($h = 0.56$) combined with the camber line D_5, it is necessary to use the thickness $e = 0.15$ in order to obtain the same magnitude of leading-edge radius, and the camber $f = 0.012$ in order to realize the optimum lift coefficient 0.15.[5] Therefore we construct an airfoil by applying the symmetrical form K with $e = 0.15$ normal to the chord around the camber line D_5 with $f = 0.012$. We call it D_5K - 1215. The angle of attack corresponding to $C_L = 0.15$ is 1.56° for NACA 23012 and 0.60° for D_5K - 1215. The pressure distribution for that condition is shown in figure 20.

We then estimate C_{D_0} for the two airfoils by the method explained previously. The results are shown by broken lines in figure 21. In order to check the results, measured values taken from various sources for the two airfoils and similar airfoils are also plotted in the same figure by different marks. The mark o refers to the value obtained by flight experiments on a smooth surface, and • refers to that obtained by wind tunnel experiments where the stream turbulence has no effect on transition. The mark + refers to the flight experiment on a rough surface, while × refers to the wind tunnel experiment where the stream turbulence causes the transition to occur prematurely. Therefore, only o and • are adequate for our present purpose. Drawing curves through these points and extrapolating to higher Reynolds numbers, we find that the result agrees fairly well with the estimated values. Therefore, we may consider that the method of estimating C_{D_0} is sufficiently accurate at the Reynolds numbers corresponding to actual flight

---

[5]The calculation developed in paragraphs 8 to 11 refers to the potential flow of an ideal fluid, so that it gives the slope of lift curve $\frac{dC_L}{d\alpha} = 2\pi$. In real fluids, however, the slope of lift curve amounts to only 80 to 90 percent of the theoretical value. If we take this effect into account, we have to increase the necessary amount of f by 10 to 20 percent in order to realize the given lift coefficient. However, such a slight change in the value of f will scarcely affect the estimation of C_{D_0}.

conditions. Comparison of two airfoils, laminar-flow and conventional, also suggests the possibility of 40 percent reduction in profile drag by using a fairly practical laminar-flow airfoil.

CONSIDERATION OF THE AIRFOIL WITH UNIFORM DISTRIBUTION OF PRESSURE

20. The fact that, so far as flight experiments with smooth wings are concerned, the boundary layer transition occurs only in the region of rising pressure, not only warrants the principle of designing the laminar-flow airfoil by shifting the minimum pressure backward, but also suggests the possibility of delaying the transition by using an airfoil with uniform distribution of pressure. Therefore, in paragraphs 21 to 23, the shape of such a symmetrical airfoil is determined by a method similar to that used for designing the camber line of laminar-flow airfoils, and the airfoil was examined by wind tunnel experiments. In paragraphs 24 to 26, a calculation is made to inquire about the method of sucking away the boundary layer over the region of rising pressure in such a way that the boundary layer velocity profile shall remain the same as that for the point of minimum pressure.

21. Consider the symmetrical airfoil set at zero angle of attack. According to the formula of paragraph 3, the pressure distribution is given by

$$\frac{p}{q} = 1 - \frac{\left[1 + 2\sum_{1}^{\infty} nb_n \frac{\sin n\xi}{\sin \xi}\right]^2}{1 + \left[2\sum_{1}^{\infty} nb_n \frac{\cos n\xi}{\sin \xi}\right]^2}$$

where p is the pressure acting on the airfoil surface, measured from the static pressure of the undisturbed stream, q is the dynamic pressure of the undisturbed stream, $x = \frac{1}{2}(1 + \cos \xi)$ is the coordinate along the chord, and the half-thickness of the airfoil is expressed in the form

$$T = \sum_{1}^{\infty} b_n \sin n\xi$$

If the thickness is sufficiently small, the square of

$$\frac{dT}{dx} = -2 \sum_{1}^{\infty} nb_n \frac{\cos n\xi}{\sin \xi}$$

may be neglected, so that the condition of uniform distribution of pressure is satisfied by putting all the coefficients b_n, other than b_1, equal to zero, namely, by an elliptic section. In order to take the thickness into account approximately, we substitute the value of dT/dx for the elliptic section into the denominator of the expression for p/q. Then, writing e for the maximum thickness in terms of the chord, we get

$$\frac{p}{q} = 1 - \frac{\left[\sin \xi + 2 \sum_{1}^{\infty} nb_n \sin n\xi\right]^2}{\sin^2\xi + e^2\cos^2\xi}$$

hence

$$2 \sum_{1}^{\infty} nb_n \sin n\xi = -\sin \xi + B\sqrt{\sin^2\xi + e^2\cos^2\xi}$$

where B is the constant value of $(1 - p/q)^{1/2}$. We have therefore

$$\sin \xi \frac{dT}{dx} = -\frac{1}{\pi}\int_0^{\pi} 2 \sum_1^{\infty} nb_n \sin n\xi' \frac{\sin \xi' \, d\xi'}{\cos \xi - \cos \xi'}$$

$$= \frac{1}{\pi}\int_0^{\pi} \left\{ \sin \xi' - B\sqrt{\sin^2 \xi' + e^2 \cos^2 \xi'} \right\} \frac{\sin \xi' \, d\xi'}{\cos \xi - \cos \xi'}$$

$$= u - \frac{B}{\pi} \left\{ 2ku \cos^{-1} e + \right.$$

$$\left. \sqrt{1 - k^2u^2} \log \frac{(1 + u)\left(1 - k^2u + e\sqrt{1 - k^2u^2}\right)}{(1 - u)\left(1 + k^2u + e\sqrt{1 - k^2u^2}\right)} \right\}$$

where

$$u = \cos \xi = 2x - 1 \qquad k = \sqrt{1 - e^2}$$

Upon integrating we get

$$T = \left\{ \frac{B}{\pi} k \cos^{-1} e - \frac{1}{2} \right\} \sqrt{1 - u^2} -$$

$$\frac{B}{2\pi}\int_{-1}^{u} \sqrt{\frac{1 - k^2u^2}{1 - u^2}} \log \frac{(1 + u)\left(1 - k^2u + e\sqrt{1 - k^2u^2}\right)}{(1 - u)\left(1 + k^2u + e\sqrt{1 - k^2u^2}\right)} du$$

The integral is evaluated by a numerical method, and the value of the constant B determined from the condition that $T = \frac{1}{2}e$ when $u = 0$. The numerical results for three values of e are given in table 8, T and dT/dx being expressed in terms of those for the elliptic section.

The shapes of the airfoils are shown in figure 22. The shape resembles an elliptic section, although it is somewhat fuller at the ends. It will also be seen that the constant B, as shown in the following table, is slightly smaller than $1 + e$, the maximum value of $(1 - p/q)^{1/2}$ for the elliptic section. Since the values of $(dT/dx) \div \left(-eu/\sqrt{1 - u^2}\right)$ are not far different from 1, it seems to be sufficiently accurate to substitute the value of dT/dx for the elliptic section into the denominator of $1 - p/q$.

e	B
0.1	1.097
.2	1.188
.3	1.273

22. The uniform distribution of pressure requires, however, an infinite pressure gradient at both leading and trailing edges. In order to see to what degree such a sharp pressure gradient may be realized in actual fluids, measurements were made on a model of the airfoil section with uniform distribution of pressure with $e = 0.1$ (we call it U.P. 0010) in the 1.5 m wind tunnel of the Aeronautical Research Institute. The model was made of laminated mahogany, of 0.8 m span, of 0.8 m chord, and fitted with end plates 1.3 m × 0.6 m. Measurements of pressure distribution, wake traverse and boundary layer transition were similar to those already mentioned in paragraphs 12 to 14.

The pressure distribution along the chord is shown in figure 23 for three values of R, the Reynolds number referred to chord length. The observed value is somewhat high compared to the theoretical value $\frac{p}{q} = -0.203$, the discrepancy probably being due to the excessive size of the model in proportion to that of the wind tunnel. At any rate, however, the pressure distribution is nearly uniform. The lack of uniformity exists at both edges due to the impossibility of realizing the infinite pressure gradient. The boundary layer separates near the trailing edge, but the effect of separation becomes small as the Reynolds number increases. This scale effect seems to be of the same nature as that responsible for the sudden drop in sphere drag; the boundary layer separates in a laminar state when the Reynolds number is low, while it becomes turbulent before separation when the Reynolds number is high, thus being able to proceed against a larger pressure gradient. This is also seen from the measurements in the wake, where the indentation of the curve of total pressure distribution is shallow and wide for low Reynolds numbers, while it becomes deep and narrow as the Reynolds number increases. As a result, the profile drag coefficient C_{D_0} decreases considerably

as the Reynolds number increases, as shown in figure 24. Transition to turbulence was found very near to the trailing edge, occurring downstream of $x = 0.9$ in the range of measurements. Measured values of the drag of the model when a piano wire of 0.5 mm diameter was placed at $x = 0.8$ and $x = 0.9$, respectively, are also plotted in the same figure. The drop in drag occurs at a lower value of the Reynolds number when the surface is roughened by the wire.

23. The profile drag coefficient of the airfoil U.P. 0010 is shown below in comparison with other symmetrical airfoils at $R = 2.2 \times 10^6$:

NACA 0010	$c_{D_0} = 0.0064$ (fig. 13)
L.B. 24	0.0032 (fig. 13)
U.P. 0010	0.0059
U.P. 0010, a wire at $x = 0.9$	0.0044

All the airfoils are of 10 percent thickness. NACA 0010 is a conventional airfoil, and L.B. 24 is a laminar-flow airfoil with far back minimum pressure. The drag of U.P. 0010 is between that of these two airfoils, the drag when a wire is placed being nearly the mean of the two. This result seems to be interesting in that the drag of an airfoil with a blunt tail is smaller than commonly considered.

The airfoil with uniform distribution of pressure will also probably be favorable when used at high subsonic speeds. Even if the shock wave occurs at high subsonic speeds, the increase in drag will remain small when the boundary layer does not separate. This expectation was really verified by the experiment due to Kawada and Kawamura (ref. 22), the drag of the airfoil U.P. 0010 being smaller at high Mach numbers as compared with other airfoils.

24. From the fact that the boundary layer transition occurs only in the region of rising pressure, we may also expect suction of the boundary layer to delay transition. For example, if the boundary layer is sucked into a slot, there is a well-known sink effect (ref. 23) which relieves the adverse pressure gradient somewhat upstream of the slot. We may consider an alternative possibility. That is, we assume that the boundary layer is laminar in the region of falling pressure, and that it remains laminar also in the region of rising pressure provided that the boundary layer profile is the same as that at the minimum pressure point. We then ask what suction arrangement must be applied in order to realize such a condition.

25. We denote by s the coordinate measured along the surface, y perpendicular to the surface, δ the boundary layer thickness, u the velocity in the boundary layer, u_1 the velocity outside the boundary

layer, $\frac{dp}{ds} = -\rho u_1 \left(du_1/ds\right)$ the pressure gradient, and $\tau_0 = -\mu \left(\partial u/\partial y\right)_{y=0}$ the skin friction at the surface. Assuming the surface ($y = 0$) is made porous, through which the fluid is sucked with the velocity c, we have the equation of continuity

$$w - c = \frac{d}{ds}\int_0^\delta u \, dy \tag{a}$$

and the equation of momentum

$$\rho u_1 w - \rho \frac{d}{ds}\int_0^\delta u^2 \, dy = \tau_0 + \delta \frac{dp}{ds} \tag{b}$$

where w is the velocity of fluid entering the boundary layer through $y = \delta$. The equation of motion reduces to

$$-c\left(\frac{\partial u}{\partial y}\right)_{y=0} = u_1 \frac{du_1}{ds} + \nu\left(\frac{\partial^2 u}{\partial y^2}\right)_{y=0} \tag{c}$$

for $y = 0$.

Now, the velocity profile in the boundary layer may be approximated by the Pohlhausen polynomial

$$u = u_1 \left\{2\frac{y}{\delta} - 2\frac{y^3}{\delta^3} + \frac{y^4}{\delta^4}\right\} \tag{d}$$

when neither pressure gradient nor suction exists. For this profile we have

$$\tau_0 = 2\mu \frac{u_1}{\delta} \tag{e}$$

$$\rho u_1 w = \frac{441}{74} \tau_0 \tag{f}$$

To simplify the calculation, we assume that the expressions (d), (e), and (f) still hold when both pressure gradient and suction exist. Then we have from (b)

$$\frac{d\delta}{ds} = \frac{630}{37}\frac{\nu}{u_1\delta} - \frac{104}{367}\frac{\delta}{u_1}\frac{du_1}{ds} \tag{g}$$

Integrating we have

$$u_1^m \frac{\delta^2}{\nu} = \left(u_1^m \frac{\delta^2}{\nu}\right)_{s=s_0} + \frac{1260}{37}\int_{s_0}^{s} u_1^{m-1}\, ds \tag{h}$$

where $m = \frac{208}{367}$, and s_0 is the initial position of suction, which is the minimum pressure point in the present case. We have also from (a)

$$c = \frac{1841}{3670}\frac{du_1}{ds}\delta \tag{i}$$

If we substitute (d) and (i) into both sides of the equation (c), however, the left and right sides become $1.003u_1\left(du_1/ds\right)$ and $u_1\left(du_1/ds\right)$, respectively. This contradiction is evidently due to the crude assumption of using (f) in spite of the presence of pressure gradient and suction, but we may overlook the error because it is small.

26. We apply the calculation to the symmetrical laminar-flow airfoil of 10 percent maximum thickness, L.B. 24, set at zero angle of attack. The velocity distribution u_1/V calculated from the potential flow of ideal fluids is used,[6] the maximum velocity (minimum pressure) being located at 64 percent of the chord from the leading edge $\left(s_0 = 0.65t\right)$. Applying a distributed suction downstream of the minimum pressure point so as to maintain the velocity profile in the boundary layer the same as at this point, we have the boundary layer thickness δ and the required

---

[6]It is assumed that the velocity distribution is not affected by the suction. Theoretically u_1 should be 0 at the trailing edge, but the distribution was somewhat modified so as to give $u_1 = 0.85V$ there. The effects of these assumptions appear to be too small to affect the result materially.

suction velocity c as shown in figure 25. It is to be noted that s is measured along the surface from the leading edge, and R is the Reynolds number based on the chord length t and the velocity of the undisturbed stream V. Integrating the area under the curve of c, we have the total amount of suction $1.3\nu\sqrt{R}$ per unit span of the two surfaces. If we assume span = 35 m, t = 5 m, V = 200 m/s, ν = 0.15 cm^2/s, the total amount of suction amounts to 5.6 m^3/s, which will require an exit area of only 0.028 m^2 when discharged with the velocity equal to V. Integration of τ_0 gives the drag coefficient $C_{D_0} = 0.0005$. This value may be compared with $C_{D_0} = 0.0003$ for the flat plate with laminar boundary layer, $C_{D_0} = 0.0044$ for the flat plate with turbulent boundary layer, and $C_{D_0} = 0.0025$ for L.B. 24 without suction. If the thickness of the airfoil is doubled (20 percent chord), then the amount of suction will be nearly doubled; the drag is however almost unchanged.

It should be noticed again that the calculation is based on the assumption that no transition occurs if the velocity profile in the boundary layer maintains the form at the minimum pressure. It is the purpose of the calculation to show that extraordinarily low profile drag may be expected with a relatively small amount of suction under such a condition.

PREMATURE TRANSITION OF BOUNDARY LAYER - EFFECT OF STREAM TURBULENCE

27. Although the transition of the boundary layer occurs only downstream of the minimum pressure, so far as flight experiments on smooth airfoil surfaces are concerned, there are many examples of wind tunnel experiments in which the transition moves upstream of the minimum pressure. This seems to be due to the premature transition caused by the turbulence in the wind tunnel stream. For example, the transition on the airfoil L.B. 24 was found only downstream of the minimum pressure in the range of Reynolds numbers covered by the author's wind tunnel experiments (the Reynolds number based on chord length up to 3×10^6; see paragraphs 12 to 14); as a result very low values of the profile drag coefficient C_{D_0} were observed. The same airfoil, however, when tested with a larger model of 2 m chord in the 2.5 m wind tunnel of Kawasaki Aircraft Company, Gihu, gave the result as shown in figure 26, in which C_{D_0} increases considerably when the Reynolds number exceeds 5×10^6 (refs. 24 and 25). There is reason to believe that the increase in drag is due to the effect of stream turbulence. The boundary layer observation at the Kawasaki wind tunnel shows that the transition is found at 50 percent chord ($x = 0.5$) for the Reynolds number 6×10^6 and moves

further forward as the Reynolds number increases. The boundary layer velocity profile observed at transition has a form factor $\frac{\delta^*}{\theta} = 2.6$ (δ^* and θ are the displacement and momentum thicknesses of the boundary layer), which is very near to the value for the case of zero pressure gradient. This result seems to suggest that the transition is at least not correlated with the laminar separation (ref. 1).

28. In order to verify this conjecture, it is desirable to show that the transition in the boundary layer along a flat plate occurs under the same condition, because that transition may be considered to be independent of the laminar separation. Unfortunately, however, no flat plate was measured in the Kawasaki wind tunnel. Therefore we proceed in a somewhat indirect way. We assume that the degree of stream turbulence is represented by the conventional critical Reynolds number of the sphere, R_C, and the condition of transition due to turbulence represented by the local Reynolds number, $R_\theta = \frac{u_1\theta}{\nu}$, at transition on a flat plate, where u_1 is the velocity outside the boundary layer and θ is the momentum thickness of the boundary layer. It is generally accepted that the turbulence in the wind tunnel stream will give a fluctuation of pressure gradient, as a result of which an instantaneous and intermittent separation will occur. Such an instantaneous and intermittent separation, however, does not necessarily lead to the transition into turbulence; for the transition really to occur, it seems probably necessary that the Reynolds number R_θ which represents the ratio of inertia ρu_1^2 to viscous stress $\rho\nu u_1/\theta$ exceed a certain critical value. It is also expected that the critical value depends on the degree of turbulence; it must increase as R_C increases. This is really shown by the experimental data hitherto published, which are given in the following table and also by white circles (o) in figure 27. The available data are scanty, especially because the experiment on a flat plate is very difficult. It was necessary for the author to perform a new experiment (ref. 30) with a view to adding one point in the range of high R_C.

R_C	R_θ	Wind Tunnel	Reference
1.40×10^5	0.21×10^3	National Bureau of Standards	26
2.75×10^5	$.70 \times 10^3$	National Bureau of Standards	26
2.20×10^5	$.42 \times 10^3$	N.P.L. Compressed Air Tunnel	27, 28
3.66×10^5	1.05×10^3	Aero. Res. Inst. 1.5 m Tunnel	29, 30

29. Now, we calculate the value of R_θ at transition of the airfoil L.B. 24 tested in the Kawasaki wind tunnel, and correlate it with the critical Reynolds number R_C of that tunnel. We analyze similarly the other available data, and summarize the result in the following table. The values of the form factor δ^*/θ, not shown, were all found in the range from 2.1 to 2.7. We then plot the data also in figure 27 by black circles (●). The black circles are seen to define a single curve together with the white circles already mentioned. This result seems to support the supposition that the transition under consideration is mainly caused by the stream turbulence, but not correlated with the laminar separation.

R_C	R_θ	Model	Wind Tunnel	Reference
1.85×10^5	0.41×10^3	Symmetrical airfoil	N.P.L. 7 ft	31, 32
2.10×10^5	$.56 \times 10^3$	Airship model	M.I.T. $7\frac{1}{2}$ ft	33, 34
3.50×10^5	$.95 \times 10^3$	Airfoil N-22	NACA Full-Scale	12, 35
3.65×10^5	1.08×10^3	Airfoil L.B. 24	Kawasaki 2.5 m	24, 25

In reference 12 (the third line in the preceding table), the same airfoil was examined both by the full-scale wind tunnel and by the flight tests. We calculate the form factor δ^*/θ from these tests and plot the values against s/t in figure 28, where t is the chord length and s is the length measured along the surface from the leading edge. The value of δ^*/θ at transition is 2.6 in the wind tunnel, while it reaches as high as 3.1 and drops sharply in the flight test. The minimum pressure is located at $\frac{s}{t} = 0.18$, and the laminar separation calculated from the measured distribution of pressure at $\frac{s}{t} = 0.36$. This example is very interesting because the cause of transition is quite different in the two cases (namely, it is due to the stream turbulence in the wind tunnel, while it is related to laminar separation in the flight test), although the positions of transition are almost the same.

PREMATURE TRANSITION OF BOUNDARY LAYER - EFFECT OF SURFACE ROUGHNESS

30. Up to this point, we have only considered the case when the surface of the airfoil is smooth. If the surface is rough, however, there is a possibility that the transition may also be caused prematurely by surface roughness. So, it is important in practice to estimate the

approximate order of magnitude of the permissible roughness in the laminar boundary layer. Nothing has been known concerning this problem, except a mere conjecture or fragmentary data. Schiller (ref. 36) suggested that a local separation occurs and hence leads to transition when the Reynolds number ku_k/ν exceeds a certain critical value R_{crit}, where k is the height of projection and u_k is the velocity at the top of projection. The exact value of R_{crit} is not known, but it is not likely to differ much from the critical value of the Reynolds number, above which vortices are shed from the obstacle of the same shape as that of the projection placed in a uniform stream. The experimental result due to Wieselsberger (ref. 37) shows that such a critical Reynolds number is roughly 50 for a circular cylinder. Assuming that the height of projection k is small, and that the presence of the projection in no way alters the character of the flow, we have the shearing stress at the surface $\tau_0 = \rho\nu(u_k/k)$. Using the so-called friction velocity $v_* = \sqrt{\tau_0/\rho}$ instead of u_k, we have then $kv_*/\nu = \sqrt{ku_k/\nu}$. The permissible roughness is therefore given by $kv_*/\nu = \sqrt{R_{crit}}$, or, with $R_{crit} = 50$, $kv_*/\nu = 7$. On the other hand, according to Nikuradse's experiments on roughened pipes (ref. 38), the critical Reynolds number is $\frac{kv_*}{\nu} = 4$, above which the roughness projections disturb the laminar sublayer of the turbulent boundary layer and hence increase the pressure drop. It appears therefore that the permissible roughness is smaller in the turbulent boundary layer as compared with the laminar boundary layer. This is confined by a British flight experiment (ref. 39) on the airfoil section of 10 feet chord (Reynolds number 1.8×10^7), because the effect of camouflage paint of 0.001 inch thickness increased the drag by about 6 percent without moving the transition forward. At any rate, however, such a estimate is nothing but mere conjecture. With a view to making the estimate more definite, we performed wind tunnel experiments, although of small scale, of quantitative character (paragraphs 31 to 32).

31. A polished aluminum plate, 80 cm long, 60 cm wide, and 3 mm thick, was held horizontally in the 1.5 m wind tunnel of the Aeronautical Research Institute. So that the flow at entry would not be disturbed, the leading edge of the plate was rounded, and the plate slightly tilted so that the forward stagnation point was on the same surface as that where the observation was made. The tilting, however, was so slight that the static pressure was observed to be practically uniform along the plate. The plate was roughened by a wire, which was stretched across the flow, in contact with the plate. The diameters k of the wire were 0.25, 0.4, and 0.7 mm, respectively, and the distances x of the wire from the leading edge were 15, 30, 45, and 60 cm, respectively. When the wind speed V was low, the boundary layer was laminar all along the plate, but from a certain speed upward, the transition to turbulent flow was observed at that point where

the wire was placed. Transition was detected by a sudden change in the value of the total pressure G^* in terms of the dynamic pressure q of the undisturbed stream, G^* being indicated by a small pitot tube with a flattened mouth of 1 mm external width and 0.3 mm width, which was placed in contact with the plate at a point 70 cm behind the leading edge. A sample record of measurements for $k = 0.4$ mm is shown in figure 29.

When a flat plate is placed along a uniform stream of velocity V, the Blasius solution (ref. 40) of the laminar boundary layer equation gives

$$v_* = 0.576V\left(\frac{Vx}{\nu}\right)^{-3/4}$$

for a point of distance x from the leading edge. Writing K for the critical value of kv_*/ν, the permissible height of projection k is given by

$$0.576\,\frac{k}{x} = K\left(\frac{Vx}{\nu}\right)^{-3/4}$$

We determine V from the wind speed corresponding to the kink of the curve as shown in figure 29, plot $0.576(k/x)$ in a logarithmic scale against Vx/ν, and draw a straight line of the slope $-3/4$ through the points (fig. 30). We thus obtain $K = 13$, which is far greater than the value $K = 7$ estimated previously.

32. Similar measurements were also performed on an airfoil section L.B. 24. The model was of 0.8 m span, of 1.2 m chord, fitted with end plates 1.3 m × 0.6 m, and set at zero angle of attack in the same wind tunnel. Wires of various diameters ($k = 0.25$, 0.4, 0.7 mm) were attached parallel to the span, in contact with the surface, at 10 percent of the chord from the leading edge ($x = 0.1$). Transition was detected by the sudden change in total pressure as indicated by a pitot tube with a flattened mouth of 2.7 mm external width and 0.9 mm depth, which was placed in contact with the surface at 50 percent of the chord from the leading edge. Results of measurements are shown in figure 31, where $R = \frac{Vt}{\nu}$, and t is the chord length.

The friction velocity may be generally expressed in the form

$$v_* = AVR^{-1/4}$$

where A is a function of s/t (s is the length measured along the surface from the forward stagnation point). We can calculate A by applying either the Pohlhausen approximate solution (ref. 41) or the simplified method due to the author (refs. 15 and 16). The permissible height of projection is then determined by

$$A \frac{k}{t} = KR^{-3/4}$$

Applying the Pohlhausen method to the theoretically calculated distribution of pressure, we get the values of function A, as shown in figure 32. Since A is 1.23 at the position of wire (x = 0.1), the value 1.23(k/t) is plotted in a logarithmic scale against R in figure 33, R being the Reynolds number corresponding to the kink of the curve as given in figure 31. It will be seen that although the measured points are on a straight line of the slope -3/4, they give K = 15, which is somewhat higher than the value found for the flat plate.

33. Now we apply the preceding result to the fragmentary data hitherto known in order to check the adequacy of the estimate. First, we examine the results of wind tunnel experiment on a symmetrical laminar-flow airfoil L.B. 27,[7] on which various projections are attached at 3 percent of the chord from the leading edge (x = 0.03). The model was of 0.8 m span, of 1.2 m chord, and set at zero angle of attack. The profile drag was measured by the method similar to that for L.B. 24 (see paragraphs 12 to 13). The results are shown in figure 34, from which we find that the rubber tape of 0.07 mm thickness gives no effect over the range of Reynolds numbers R covered by the experiment, while the piano wire of 0.5 mm diameter gives a completely turbulent friction. The effect of the wire of 0.25 mm diameter begins to appear at $R = 1.3 \times 10^6$. Inserting the values k = 0.25 mm, t = 1.2 m and A = 1.95 in the formula $A \frac{k}{t} = KR^{-3/4}$, we get K = 15.5, which is in good agreement with the result in paragraph 32. The value A = 1.95 was read from figure 32, since the leading edge portion of L.B. 27 almost coincides with that of L.B. 24. Profile drag coefficients of both airfoils are also the same over the range of Reynolds numbers examined.

34. In connection with the determination of boundary layer transition on airfoils in the NACA full-scale wind tunnel (ref. 42), an auxiliary measurement has been reported, in which the effect was examined

---

[7] L.B. 27 has a maximum thickness of 10 percent of the chord at 60 percent of the chord from the leading edge. See figure 5 of paragraph 6.

of rubber tapes attached at 5 percent of the chord ($x = 0.05$) from the leading edge of the model. The airfoil section was NACA 0012, the chord was 72 inches, and the Reynolds number R was 4.18×10^6. No effect was found when the tape was 0.003 inch thick, some effect began to appear when it was 0.006 inch thick, and the transition moved right to that position where the tape of 0.009 inch thickness was attached. Assuming $A = 1.6$ and $K = 15$, we estimate from the preceding formula the value 0.007 inch for the permissible thickness, which seems to agree well with the observation.

If we further assume that the value $A = 1.6$ is also applicable to the case of the British flight experiment mentioned in paragraph 30, we find 0.004 inch for the critical height for transition with $t = 10$ feet, $R = 1.8 \times 10^7$, and $K = 15$. On the other hand, we estimate the permissible limit in turbulent boundary layer by $\frac{kv_*}{\nu} = 4$, which may be written in the form

$$\frac{k}{t} = \sqrt{\frac{2}{c_f}} \frac{V}{u_1} \frac{4}{R}$$

by the relation $v_*^2 = \frac{1}{2} c_f u_1^2$, where u_1 is the local wind speed and c_f is the coefficient of local skin friction. If we assume $u_1 = 1.2V$ and $c_f = 0.003$ (which is equal to the coefficient of mean skin friction for a flat plate at $R = 1.8 \times 10^7$), we obtain 0.0006 inch for the permissible roughness thickness. Since the thickness of the camouflage paint is reported to be about 0.001 inch, it may be concluded that the paint increases only the friction in turbulent boundary layer, without affecting, however, the transition to turbulent flow. This is in good agreement with the experimental results.

APPENDIX

TRANSITION CAUSED BY LAMINAR SEPARATION

35. As is well-known, the phenomenon of sudden decrease in drag of a sphere at a certain value of the Reynolds number $R = \frac{Vd}{\nu}$ (V is the speed of undisturbed stream and d is the diameter of sphere) is explained by supposing that the boundary layer separates while it is laminar when R is low, but it separates after transition to turbulence when R is high, thus resulting in diminishing the so-called dead water region. Probably the transformation from laminar separation to turbulent separation may proceed as follows:

When the laminar boundary layer separates from the surface, the detached layer remains also laminar at first, but it is so unstable that it becomes turbulent at a short distance. This transition from laminar to turbulent flow is considered to occur when the local Reynolds number based on the width of the detached layer and the velocity outside the layer exceeds a certain value, so that the transition moves upstream toward the separation point as R increases. When the transition approaches sufficiently near the separation point, it becomes possible for the detached layer to come back again to the downstream surface, because the turbulence produced will drive the flow forward. The layer reattaches to the surface as a turbulent layer, and accordingly the drag coefficient begins to decrease. The distance between the separation and the first turbulent boundary layer decreases as R increases, and finally the fully developed turbulent boundary layer commences just downstream of the separation point. The drag coefficient then ceases to decrease.

36. Now, in order that the separated layer reattach to the surface, it seems necessary for the local Reynolds number $R_\theta = \frac{u_1\theta}{\nu}$ at separation to exceed a certain critical value, where u_1 is the velocity outside the boundary layer, and θ is the momentum thickness of the boundary layer. This may be explained as follows: According to the laminar boundary layer theory, the separation occurs when the quantity

$$-\frac{\theta^2}{\nu}\frac{du_1}{ds} = \frac{dp}{ds}\theta \div \rho\nu\frac{u_1}{\theta}$$

exceeds a certain value, suggesting that the pressure rise $(dp/ds)\theta$ becomes too large in proportion to the shearing stress at the surface $\rho\nu(u_1/\theta)$. Assuming analogically that the separated layer leaves

the surface when the pressure rise becomes too large in proportion to the momentum ρu_1^2, we then find that R_θ at the separation point must exceed a certain critical value in order that the separated layer reattach to the surface.

37. In order to determine the critical value of R_θ, we consider in detail the condition where the coefficient of sphere drag begins to decrease. This condition corresponds to the point B of the curve of figure 35, which represents an idealized variation of the drag coefficient $C_D \left[= \text{drag} \div \left(\rho V^2/2\right)\left(\pi d^2/4\right)\right]$ or the pressure difference coefficient $\Delta p/q \left[= \text{difference of pressures at the forward stagnation point and the point corresponding to the central angle } 157.5^\circ \div \left(\rho V^2/2\right)\right]$ with the Reynolds number R. Within the range AB, the pressure distribution around the sphere is approximately independent of R; the typical example may be found from the experiments due to Fage (ref. 43). Fortunately, the boundary layer calculation has also been performed for that distribution of pressure by Tomotika and Imai (ref. 44), so that the local Reynolds number R_θ is given by

$$R_\theta = 0.40\sqrt{R}$$

at the separation point. Although the calculation has originally been made for a particular Reynolds number, $R = 1.57 \times 10^5$, the preceding relation may be applied for any value of R in the range of AB. Putting the value of R at B, and writing

$$R_{\theta_{crit}} = 0.40\sqrt{R_B}$$

we have $R_{\theta_{crit}}$ as the critical value of R_θ above which the separated laminar layer reattaches to the surface. Conventionally the Reynolds number R_C corresponding to $C_D = 0.3$ (or $\Delta p/q = 1.22$) has been used, instead of R_B, for representing the degree of stream turbulence, but it is not so difficult to estimate the value of R_B from the measured curve of C_D (or $\Delta p/q$) against R. For example, we have from the experiments of towing spheres in the free atmosphere (ref. 35)

$$R_B = 3.6 \times 10^5 \qquad R_C = 3.85 \times 10^5 \qquad R_{\theta_{crit}} = 240$$

Since these values refer to the case of very low turbulence, it will be seen that $R_{\theta_{crit}} = 240$ represents the highest possible value. It is also to be noted that $\frac{R_B}{R_C} = 0.94$ in this example and that almost the same value has been obtained by the author's experiments on spheres of various diameters (ref. 29).

38. If the stream turbulence is not low so that R_C is less than 3.85×10^5, then $R_{\theta_{crit}}$ will be less than 240. Assuming the ratio R_B/R_C to be constant, we can estimate the corresponding value by

$$R_{\theta_{crit}} = 240\sqrt{\frac{R_C}{3.85 \times 10^5}}$$

On the other hand, we can also estimate the value of $R_{\theta_{crit}}$ directly from the boundary layer measurements. The results of the analysis for a sphere as well as circular and elliptic cylinders are summarized in the following table, where $R_{\theta_{crit}}$ is the critical value R_θ estimated from R_C by the preceding formula, $R_{\theta_{sep}}$ is the value of R_θ observed at the separation point when the boundary layer really separates while it is laminar, and $R_{\theta_{trans}}$ is the value of R_θ observed at the calculated laminar separation point when the boundary layer separates after transition. The fact that $R_{\theta_{crit}}$ lies between $R_{\theta_{sep}}$ and $R_{\theta_{trans}}$ seems to suggest the adequacy of the preceding consideration.

Body	R_C	$R_{\theta_{crit}}$	$R_{\theta_{sep}}$	$R_{\theta_{trans}}$	Reference
Sphere	2.5×10^5	190	160	220	43
Circular cylinder	1.5×10^5	150	140	225	45
Elliptical cylinder	2.7×10^5	200	160	400	46, 47

39. We now proceed to apply our result to interpreting the effect of Reynolds number on maximum lift of airfoils. For the angle of attack near the stall, the flow separates shortly downstream of the leading edge while the boundary layer is laminar. If the flow fails to reattach to the surface as a turbulent layer, the maximum lift coefficient $C_{L_{max}}$ of

the airfoil will be almost independent of the Reynolds number R. At the separation point, similar to the case of a sphere, the relation of the form

$$R_\theta = k\sqrt{R}$$

holds, where $R = \frac{Vt}{\nu}$ is the Reynolds number referred to chord length t,[8] and k is a constant depending on the shape of airfoil and the value of $C_{L_{max}}$. If R is low so that R_θ is less than the critical value $R_{\theta_{crit}}$ then $C_{L_{max}}$ will be independent of R. Assuming the same value of $R_{\theta_{crit}}$ for the sphere as for the airfoil, we obtain

$$R = \frac{0.16}{k^2} R_B$$

for the Reynolds number above which $C_{L_{max}}$ begins to increase with the Reynolds number. Therefore, the ratio of the Reynolds number corresponding to a certain value of $C_{L_{max}}$ of an airfoil and the critical Reynolds number of sphere in the same stream, R_B or R_C, becomes independent of the stream turbulence. Denoting the values for a reference tunnel with asterisk, we have

$$\frac{R^*}{R} = \frac{R_C{}^*}{R_C}$$

which in turn means that the ratio of Reynolds numbers corresponding to a certain value of $C_{L_{max}}$ is equal to the ratio of critical Reynolds numbers of a sphere. This is useful for comparing the values of $C_{L_{max}}$ obtained in two different wind tunnels. Considering the reference condition to be the free flight in the atmosphere, we find

$$R^* = R \times \frac{R_C{}^*}{R_C}$$

---

[8]It is to be noted that R is referred to t, while R_B and R_C are referred to d.

as the free flight Reynolds number which will give the same value of $C_{L_{max}}$ as that observed in a wind tunnel. This is just what is called the effective Reynolds number. Strictly speaking, such an argument as mentioned before should apply only to the Reynolds numbers near the critical value, but there are many experimental evidences showing the usefulness of the concept of effective Reynolds number for most practical purposes, as far as the commonly used airfoils and range of Reynolds numbers of both wind tunnel and free flight are concerned.

40. Finally, we consider a more quantitative example to show the adequacy of the preceding argument. In figure 36, $C_{L_{max}}$ for various NACA symmetrical airfoils are plotted against the effective Reynolds number R^*, the experimental data being taken from the results of the NACA variable-density wind tunnel (ref. 48). As already mentioned, up to a certain value of R^*, $C_{L_{max}}$ is almost independent of R^*. This corresponds to the condition in which the laminar separation just behind the leading edge fails to reattach to the surface, resulting in a considerable dead water region above the airfoil surface. The value of $C_{L_{max}}$ is approximately 0.9, irrespective of the thickness; it is almost equal to the value for a flat plate of vanishing thickness. Theory of discontinous flow, when applied to the flat plate, seems to give a lift coefficient close to 0.9 (ref. 49). We idealize, therefore, the experimental curve as shown by dotted lines in figure 36. Then, the point where the dotted line meets the line $C_{L_{max}} = 0.9$ will be considered to correspond to $R_{\theta_{crit}} = 240$. In order to determine this point, we calculate the value of $R_\theta/\sqrt{R}$ at the laminar separation point for a lift coefficient $C_L = 0.9$, and the value of R which gives $R_\theta = 240$. We first calculate the pressure distribution by the formula of paragraph 3 for the two-dimensional potential flow around the airfoil section. Although the formula may be applied to any arbitrary airfoil section, we have determined the pressure distribution only for the airfoil

$$T = 0.287e\sqrt{x(1 - x)}(5 - 4x)$$

in order to simplify the calculation, because no great exactitude is required in the present problem. x is the coordinate along the chord, $x = 0$ and $x = 1$ corresponding to the leading and trailing edges, respectively, T is the half-thickness, and e is the maximum thickness in terms of chord length. The airfoil represented by the preceding expression coincides with sufficient accuracy with the true NACA symmetrical airfoil except near the trailing edge. The value of $R_\theta/\sqrt{R}$ at the laminar separation point was then determined for the calculated pressure distribution by applying the approximate method due to the author (refs. 15 and 16).

The critical values R^*_{crit} thus calculated are shown by a solid line in figure 37, while the corresponding values taken from figure 36 are shown by white circles. The agreement is fairly good, and especially satisfactory when the thickness of the airfoil is small. In general, the thickness of the boundary layer near the trailing edge increases as C_L increases. If C_L is further increased, however, a laminar separation suddenly occurs near the leading edge when the thickness is small, while the trailing-edge turbulent separation moves a considerable extent forward before the leading-edge laminar separation occurs when the thickness is moderate. Therefore, the assumption of the analysis is more satisfactorily realized in the case of small thickness, thus bringing the calculated and observed values in close agreement.

In conclusion, the author wishes to acknowledge his indebtedness for the assistance given by Messrs. C. Noda, S. Mituisi, I. Shinra, S. Asaka, R. Hama, and K. Takeda.

Translation by Itiro Tani
University of Tokyo
Tokyo, Japan

REFERENCES

1. Tani, I.: On the Interplay Between the Laminar Separation and the Transition to Turbulent in the Boundary Layer (in Japanese). Jour. Soc. Aero. Sci. Japan, vol. 6, 1939.

2. Tani, I.: On the Transition Caused by Laminar Separation of the Boundary Layer (in Japanese). Jour. Soc. Aero. Sci. Japan, vol. 7, 1940.

3. Tani, I., and Noda, C.: Design of Symmetrical Airfoils in Which the Minimum Pressure Occurs Well Downstream (in Japanese). Jour. Aero. Res. Inst., Tokyo Imperial Univ., nos. 190 and 193, 1940.

4. Tani, I., and Mituisi, S.: Contributions to the Design of Aerofoils Suitable for High Speeds. Rep. Aero. Res. Inst., Tokyo Imperial Univ., no. 198, 1940.

5. Tani, Itiro, Hama, Ryosuke, and Mituisi, Satosi: On the Permissible Roughness in the Laminar Boundary Layer. Rep. no. 199 (vol. XV, 13), Aero. Res. Inst., Tokyo Imperial Univ., Oct. 1940.

6. Tani, I., and Mituisi, S.; Wind Tunnel Experiments on the Airfoil U.P. 0010 (in Japanese). Jour. Aero. Res. Inst., Tokyo Imperial Univ. no. 205, 1941.

7. Tani, I.: A Simple Calculation on Boundary Layer Suction (in Japanese). Jour. Soc. Aero. Sci. Japan, vol. 8, 1941.

8. Stüper, J.: Untersuchung von Reibungsschichten am fliegenden Flugzeug. Luftfahrtforschung, vol. 11, 1934, p. 26.

9. Jones, B. Melvill: Flight Experiments on the Boundary Layer. Jour. Aero. Sci., vol. 5, no. 3, Jan. 1938, pp. 81-94.

10. Serby, J. E., Morgan, M. B., and Cooper, E. R.: Flight Tests on the Profile Drag of 14 Percent and 25 Percent Thick Wings. R. & M. No. 1826, British A.R.C., 1937.

11. Bicknell, Joseph: Determination of the Profile Drag of an Airplane Wing in Flight at High Reynolds Numbers. NACA Rep. 667, 1939.

12. Goett, Harry J., and Bicknell, Joseph: Comparison of Profile-Drag and Boundary-Layer Measurements Obtained in Flight and in the Full-Scale Wind Tunnel. NACA TN 693, 1939.

13. Moriya, T.: A Simple Method of Calculating the Aerodynamic Characteristics of an Arbitrary Wing Section (in Japanese). Jour. Soc. Aero. Sci. Japan, vol. 5, 1938, p. 7.

14. Jacobs, Eastman N., Ward, Kenneth E., and Pinkerton, Robert M.: The Characteristics of 78 Related Airfoil Sections From Tests in the Variable-Density Wind Tunnel. NACA Rep. 460, 1933.

15. Tani, I.: A Simplified Boundary-Layer Calculation for Laminar Separation (in Japanese). Jour. Aero. Res. Inst., Tokyo Imperial Univ., no. 199, 1941.

16. Tani, I.: On the Laminar Boundary Layer in Compressible Fluids (in Japanese). Rep. Aero. Res. Inst., Tokyo Imperial Univ., no. 251, 1943.

17. Theodorsen, Theodore: On the Theory of Wing Sections With Particular Reference to the Lift Distribution. NACA Rep. 383, 1931.

18. The Cambridge University Aeronautics Laboratory: The Measurement of Profile Drag by the Pitot-Traverse Method. R. & M. No. 1688, British A.R.C., 1936.

19. Shinra, I.: Flight Experiments on Laminar-Flow Airfoil (in Japanese). Paper presented at the Eighth Conference of Wind Tunnel and Water Basin Researches, Navy Aeronautical Technical Arsenal, 1940.

20. Buri, A.: Eine Berechnungsgrundlage für die turbulente Grenzschicht bei beschleunigter und verzögerter Grundströmung. Dissertation, Zürich 1931.

21. Squire, H. B., and Young, A. D.: The Calculation of the Profile Drag of Aerofoils. R. & M. No. 1838, British A.R.C., 1938.

22. Kawada, S., and Kawamura, R.: High-Speed Wind Tunnel Experiments on Airfoils U.P. 0010 and NACA 0009 (in Japanese). Jour. Aero. Res. Inst., Tokyo Imperial Univ., no. 205, 1941.

23. Schrenk, O.: Versuche mit Absaugeflügeln. Luftfahrtforschung, vol. 12, 1935, p. 10.

24. Yamashita, H.: On the Kawasaki 2.5 m Wind Tunnel (in Japanese). Jour. Soc. Aero. Sci. Japan, vol. 6, 1938, p. 29.

25. Yamashita, H., Asaka, S., Morioka, K., and Oue, M.: Wind Tunnel Experiments on the Airfoil L.B. 24 (in Japanese). Research Report of the Kawasaki Aircraft Company, vol. 2, 1941, p. 193.

26. Dryden, Hugh L.: Air Flow in the Boundary Layer Near a Plate. NACA Rep. 562, 1936.

27. Jones, R., and Williams, D. H.: The Profile Drag of Aerofoils at High Reynolds Numbers in the Compressed Air Tunnel. R. & M. No. 1804, British A.R.C., 1937.

28. Fage, A., and Williams, D. H.: Critical Reynolds Numbers of Spheres in the Compressed Air Tunnel. R. & M. No. 1832, British A.R.C., 1938.

29. Tani, I., and Hama, R.: Experiments on Pressure Spheres in the 1.5 m Wind Tunnel (in Japanese). Jour. Aero. Res. Inst., Tokyo Imperial Univ., no. 188, 1940.

30. Tani, I., Hama, R., Mituisi, S., and Iriyama, T.: Boundary Layer Measurements on a Flat Plate in the 1.5 m Wind Tunnel (in Japanese). Jour. Aero. Res. Inst., Tokyo Imperial Univ., no. 189, 1940.

31. Fage, A., and Falkner, V. M.: An Experimental Determination of the Intensity of Friction on the Surface of an Aerofoil. R. & M. No. 1315, British A.R.C., 1931.

32. Fage, A.: On Reynolds Numbers of Transition. R. & M. No. 1765, British A.R.C., 1937.

33. Lyon, Hilda M.: Effect of Turbulence on Drag of Airship Models. R. & M. No. 1511, British A.R.C., 1933.

34. Lyon, H. M.: Flow in the Boundary Layer of Streamline Bodies. R. & M. No. 1622, British A.R.C., 1934.

35. Platt, Robert C.: Turbulence Factors of NACA Wind Tunnels As Determined by Sphere Tests. NACA Rep. 558, 1936.

36. Schiller, L.: Handbuch der Experimentalphysik, vol. 4, part 4, 1932, p. 191.

37. Wieselsberger, C.: Neuere Feststellung über die Gesetze des Flüssigkeitsund Luftwiderstandes. Phys. Zeit., vol. 22, 1921, pp. 321-328.

38. Nikuradse, J.: Strömungsgesetze in rauhen Rohren. Forschungsheft 361, Beilage zu Forschung auf dem Gebiete des Ingenieurwesens, Ausg. B, Bd. 4, July-Aug. 1933.

39. Young, A. D.: Surface Finish and Performance. Aircraft Engng., vol. 11, 1939, p. 339.

40. Blasius, H.: Grenzschichten in Flüssigkeiten mit kleiner Reibung. Z.f. Math. u. Phys., vol. 56, no. 1, 1908, pp. 1-37.

41. Pohlhausen, K.: Zur näherungsweisen Integration der Differential gleichung der laminaren Grenzschicht. Z.f.a.M.M., vol. 1, 1921, pp. 252-268.

42. Silverstein, Abe, and Becker, John V.: Determination of Boundary-Layer Transition on Three Symmetrical Airfoils in the NACA Full-Scale Wind Tunnel. NACA Rep. 637, 1939.

43. Fage, A.: Experiments on a Sphere at Critical Reynolds Numbers. R. & M. No. 1766, British A.R.C., 1936.

44. Tomotika, S., and Imai, I.: On the Transition From Laminar to Turbulent in the Flow of the Boundary Layer of a Sphere. Rep. Aero. Res. Inst., Tokyo Imperial Univ., no. 167, 1938.

45. Fage, A., and Falkner, V. M.: Further Experiments on the Flow Around a Circular Cylinder. R. & M. No. 1369, British A.R.C., 1931.

46. Schubauer, G. B.: Air Flow in a Separating Laminar Boundary Layer. NACA Rep. 527, 1935.

47. Schubauer, G. B.: Air Flow in the Boundary Layer of an Elliptic Cylinder. NACA Rep. 652, 1939.

48. Jacobs, Eastman N., and Sherman, Albert: Airfoil Section Characteristics As Affected by Variations of the Reynolds Number. NACA Rep. 586, 1937.

49. Müller, W.: Einführung in die Theorie der zähen Flüssigkeiten. Leipzig 1932, section 79.

TABLE 1.- ORDINATES FOR SYMMETRICAL SECTION. VALUES OF T/e

x	I	J	K	L	M	N
0	0	0	0	0	0	0
.003	.0465	.0563	.0574	.0584	.0606	.0627
.006	.0661	.0793	.0808	.0823	.0854	.0886
.0125	.0962	.1135	.1158	.1180	.1226	.1275
.025	.1374	.1589	.1620	.1652	.1720	.1794
.05	.1963	.2208	.2252	.2298	.2396	.2508
.075	.2414	.2663	.2716	.2771	.2892	.3031
.10	.2789	.3029	.3089	.3151	.3288	.3447
.15	.3394	.3599	.3667	.3738	.3893	.4072
.20	.3865	.4026	.4097	.4170	.4328	.4503
.25	.4236	.4353	.4422	.4492	.4638	.4788
.30	.4523	.4601	.4663	.4724	.4844	.4949
.35	.4737	.4783	.4833	.4881	.4962	.5000
.40	.4885	.4906	.4942	.4971	.5000	.4953
.45	.4972	.4977	.4994	.5000	.4948	.4818
.50	.5000	.5000	.4994	.4931	.4797	.4604
.55	.4970	.4944	.4873	.4781	.4558	.4320
.60	.4871	.4778	.4656	.4522	.4241	.3975
.65	.4691	.4509	.4342	.4175	.3856	.3578
.70	.4418	.4139	.3939	.3751	.3413	.3138
.75	.4038	.3675	.3455	.3258	.2921	.2664
.80	.3538	.3121	.2899	.2706	.2393	.2165
.85	.2908	.2481	.2277	.2105	.1836	.1650
.90	.2133	.1762	.1598	.1464	.1262	.1128
.95	.1201	.0966	.0870	.0793	.0680	.0609
1.00	.0100	.0100	.0100	.0100	.0100	.0100

TABLE 2.- AUXILIARY FUNCTION B_s ASSOCIATED WITH THE PRESSURE DISTRIBUTION OF SYMMETRICAL SECTIONS

x	I	J	K	L	M	N
0.0125	0.59	1.10	1.13	1.16	1.20	1.24
.025	.66	1.06	1.09	1.13	1.20	1.26
.05	.75	1.04	1.07	1.11	1.20	1.29
.10	.86	1.03	1.07	1.11	1.21	1.33
.20	.96	1.03	1.08	1.12	1.22	1.36
.30	1.02	1.04	1.09	1.14	1.23	1.33
.40	1.05	1.05	1.10	1.15	1.23	1.22
.50	1.08	1.17	1.19	1.19	1.14	1.04
.60	1.12	1.18	1.11	1.05	.92	.80
.70	1.09	.98	.88	.79	.63	.51
.80	.89	.65	.52	.42	.28	.19
.90	.33	.06	-.03	-.10	-.18	-.22
.95	-.32	-.47	-.50	-.52	-.53	-.52
.975	-.95	-.93	-.91	-.89	-.84	-.78

TABLE 3.- AUXILIARY FUNCTION B_c ASSOCIATED WITH THE PRESSURE DISTRIBUTION OF SYMMETRICAL SECTIONS

x	I	J	K	L	M	N
0.0125	-4.04	-4.40	-4.88	-4.90	-5.20	-5.30
.025	-2.86	-3.08	-3.20	-3.22	-3.37	-3.55
.05	-2.04	-2.08	-2.13	-2.17	-2.28	-2.39
.10	-1.39	-1.33	-1.35	-1.37	-1.42	-1.48
.20	-.83	-.74	-.74	-.74	-.74	-.70
.30	-.50	-.43	-.41	-.39	-.31	-.21
.40	-.24	-.19	-.17	-.12	.00	.18
.50	.00	.00	.11	.22	.39	.50
.60	.27	.44	.53	.60	.70	.75
.70	.65	.83	.89	.92	.94	.91
.80	1.11	1.19	1.18	1.15	1.09	1.02
.90	1.70	1.52	1.41	1.31	1.16	1.04
.95	2.03	1.66	1.50	1.36	1.16	1.03
.975	2.20	1.73	1.54	1.38	1.15	1.02

TABLE 4.- ORDINATES FOR MEAN CAMBER LINES. VALUES OF M/f

x	D_0	D_1	D_3	D_5	D_∞	E_4	F_3
0	0	0	0	0	0	0	0
.003	.0295	.0282	.0292	.0300	.0371	.0313	.0327
.006	.0529	.0509	.0526	.0540	.0666	.0564	.0589
.0125	.0969	.0914	.0969	.0995	.1220	.1039	.1081
.025	.1687	.1636	.1695	.1740	.2119	.1814	.1887
.050	.2864	.2797	.2897	.2973	.3585	.3093	.3212
.075	.3843	.3772	.3907	.4006	.4787	.4161	.4315
.10	.4690	.4620	.4784	.4902	.5808	.5084	.5266
.15	.6098	.6045	.6252	.6396	.7443	.6615	.6831
.20	.7219	.7191	.7424	.7579	.8638	.7812	.8041
.25	.8113	.8112	.8353	.8507	.9451	.8733	.8952
.30	.8813	.8838	.9067	.9207	.9898	.9387	.9586
.35	.9341	.9384	.9579	.9688	.9963	.9826	.9939
.40	.9710	.9758	.9892	.9953	.9589	.9998	.9973
.45	.9928	.9962	1.0000	.9988	.8625	.9872	.9679
.50	1.0000	.9988	.9881	.9761	.6300	.9387	.9085
.55	.9928	.9813	.9472	.9178	.3885	.8561	.8238
.60	.9710	.9414	.8735	.8192	.2646	.7473	.7204
.65	.9341	.8794	.7704	.6903	.1811	.6259	.6056
.70	.8813	.7878	.6459	.5474	.1207	.4918	.4871
.75	.8113	.6898	.5108	.4078	.0772	.3682	.3721
.80	.7219	.5673	.3766	.2847	.0459	.2590	.2669
.85	.6098	.4305	.2535	.1846	.0242	.1686	.1761
.90	.4690	.2845	.1493	.1071	.0101	.0973	.1020
.95	.2864	.1366	.0651	.0472	.0024	.0425	.0442
1.00	0	0	0	0	0	0	0
x for M/f = 1	.500	.482	.450	.433	.333	.406	.381

TABLE 5.- AUXILIARY FUNCTION A_c ASSOCIATED WITH THE PRESSURE DISTRIBUTION OF MEAN CAMBER LINES

x	D_0	D_1	D_3	D_5	D_∞	E_4	F_3
0.0125	4.53	-0.53	-2.50	-3.17	-5.49	-3.51	-3.62
.025	4.53	.88	-.47	-.91	-2.17	-1.07	-1.08
.05	4.53	1.89	.99	.71	.22	.67	.74
.10	4.53	2.61	2.03	1.88	1.94	1.93	2.05
.20	4.53	3.15	2.80	2.75	3.20	2.85	3.01
.30	4.53	3.40	3.17	3.15	3.79	3.29	3.46
.40	4.53	3.56	3.40	3.41	4.18	3.57	3.61
.50	4.53	3.68	3.57	3.61	4.46	3.50	3.10
.60	4.53	3.61	3.21	2.95	-1.03	2.35	2.14
.70	4.53	3.19	2.07	1.31	-.83	1.00	1.04
.80	4.53	2.43	.75	.05	-.63	.03	.17
.90	4.53	1.34	-.05	-.26	-.42	-.26	-.22
.90	4.53	.68	-.15	-.20	-.29	-.21	-.21
.975	4.53	.33	-.08	-.14	-.20	-.15	-.15

TABLE 6.- AUXILIARY FUNCTION A_s ASSOCIATED WITH THE PRESSURE DISTRIBUTION OF MEAN CAMBER LINES

x	D_0	D_1	D_3	D_5	D_∞	E_4	F_3
0.0125	-6.31	-6.13	-6.35	-6.52	-7.92	-6.79	-7.07
.025	-5.28	-5.18	-5.37	-5.50	-6.61	-5.73	-5.94
.05	-4.25	-4.21	-4.36	-4.46	-5.25	-4.63	-4.79
.10	-3.17	-3.19	-3.29	-3.36	-3.78	-3.46	-3.55
.20	-1.99	-2.05	-2.09	-2.10	-2.00	-2.11	-2.11
.30	-1.21	-1.27	-1.22	-1.18	-.52	1.09	-.99
.40	-.58	-.58	-.43	-.31	1.26	-.07	.26
.50	0	.14	.50	.76	∞	1.33	1.46
.60	.58	1.02	1.79	2.32	2.00	2.38	2.21
.70	1.21	1.90	2.63	2.87	1.02	2.30	2.36
.80	1.99	2.61	2.60	2.24	.52	2.00	1.97
.90	3.17	2.97	1.88	1.35	.21	1.25	1.31
.95	4.25	2.91	1.63	1.05	.10	.91	1.01
.975	5.28	2.75	1.59	.94	.05	.82	.88

TABLE 7.- PRESSURE DIFFERENCE DISTRIBUTION G FOR MEAN CAMBER LINES

x	D_0	D_1	D_3	D_5	D_∞	E_4	F_3
0.0125	4.53	4.22	4.34	4.47	5.72	4.70	4.93
.025	4.53	4.22	4.34	4.47	5.72	4.70	4.93
.05	4.53	4.22	4.34	4.47	5.72	4.70	4.93
.10	4.53	4.22	4.34	4.47	5.72	4.70	4.93
.20	4.53	4.22	4.34	4.47	5.72	4.70	4.93
.30	4.53	4.22	4.34	4.47	5.72	4.70	4.93
.40	4.53	4.22	4.34	4.47	5.72	4.70	4.78
.50	4.53	4.22	4.34	4.47	5.72	4.42	4.06
.60	4.53	4.05	3.84	3.65	0	3.10	2.92
.70	4.53	3.54	2.57	1.87	0	1.60	1.67
.80	4.53	2.70	1.14	.48	0	.49	.65
.90	4.53	1.52	.20	.03	0	.05	.11
.95	4.53	.80	.03	.00	0	.00	.02
.975	4.53	.41	.00	.00	0	.00	.00

TABLE 8.- AIRFOIL WITH UNIFORM DISTRIBUTION OF PRESSURE

x	u	$T \div \frac{e}{2}\sqrt{1-u^2}$			$\frac{dT}{dx} \div \left(-\frac{eu}{\sqrt{1-u^2}}\right)$			u	x
		e = 0.1	e = 0.2	e = 0.3	e = 0.1	e = 0.2	e = 0.3		
0.00625	-0.9875	1.393	1.671	1.898	0.993	1.089	1.204	0.9875	0.99375
.0125	-.975	1.274	1.485	1.670	.955	.982	1.033	.975	.9875
.025	-.95	1.180	1.328	1.468	.934	.911	.913	.95	.975
.050	-.90	1.109	1.204	1.298	.923	.870	.830	.90	.950
.075	-.85	1.076	1.145	1.214	.919	.855	.798	.85	.925
.10	-.80	1.057	1.109	1.163	.917	.847	.780	.80	.90
.15	-.70	1.035	1.066	1.100	.915	.839	.762	.70	.85
.20	-.60	1.022	1.042	1.064	.915	.835	.753	.60	.80
.25	-.50	1.013	1.026	1.040	.914	.833	.748	.50	.75
.30	-.40	1.008	1.015	1.024	.914	.831	.744	.40	.70
.40	-.20	1.002	1.004	1.006	.913	.830	.741	.20	.60
.50	0	1.000	1.000	1.000	.913	.830	.740	0	.50

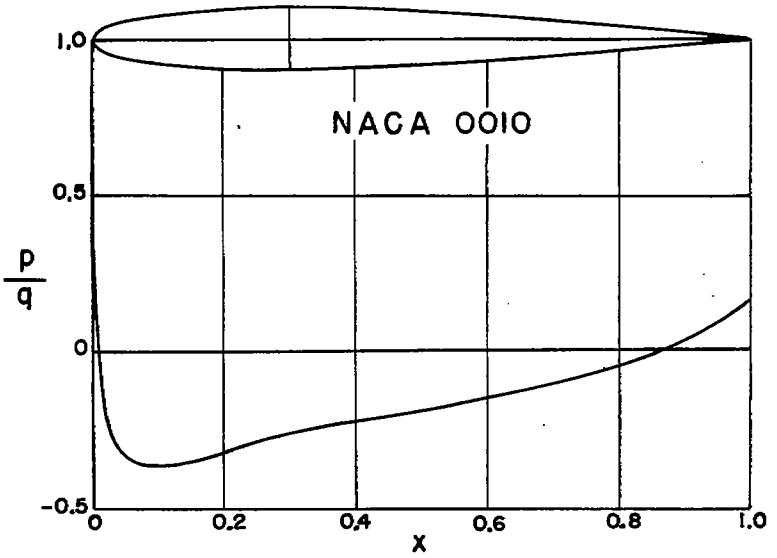

Figure 1

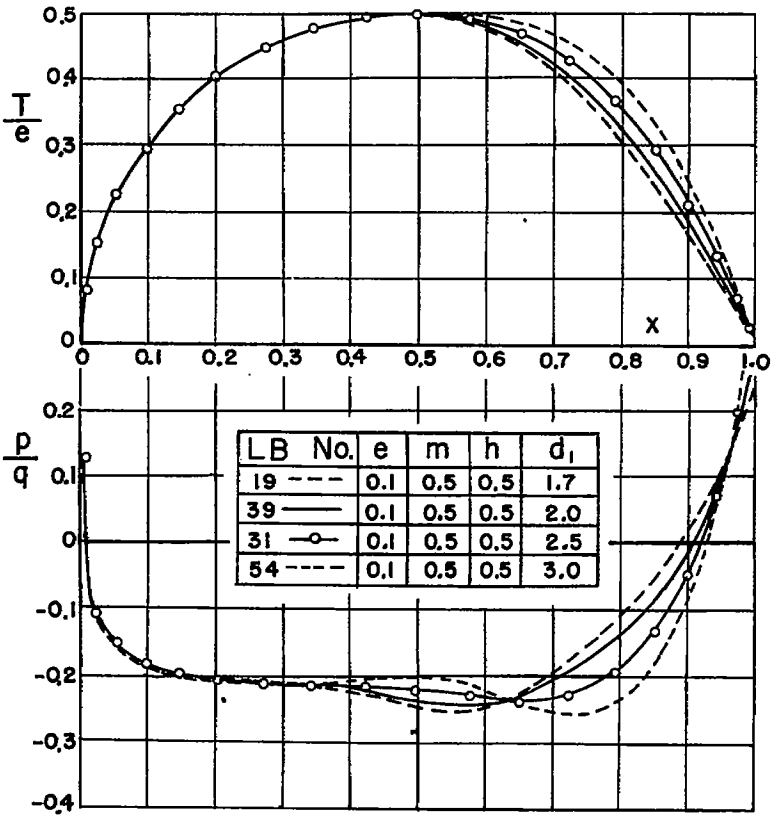

Figure 2

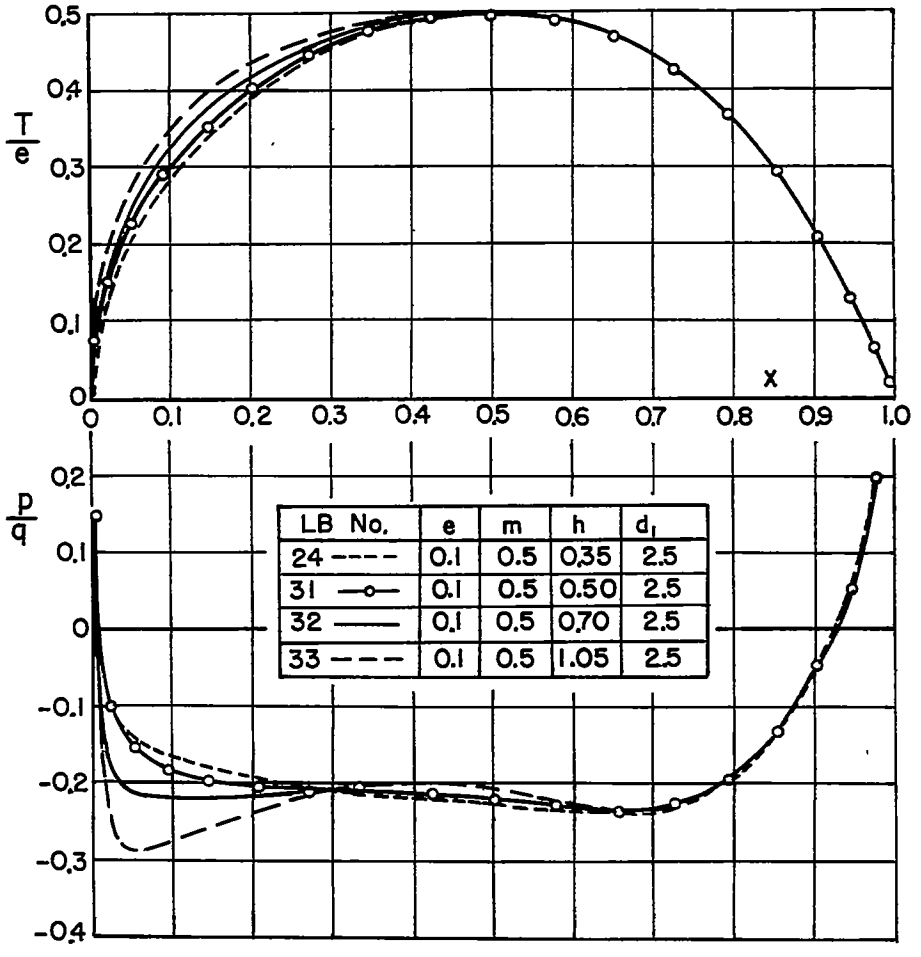
T/e
0.5
0.4
0.3
0.2
0.1
0
0 0.1 0.2 0.3 0.4 0.5 0.6 0.7 0.8 0.9 1.0
x
p/q
0.2
0.1
0
-0.1
-0.2
-0.3
-0.4
LB No. e m h d1
24 ---- 0.1 0.5 0.35 2.5
31 —o— 0.1 0.5 0.50 2.5
32 —— 0.1 0.5 0.70 2.5
33 – – – 0.1 0.5 1.05 2.5

Figure 3

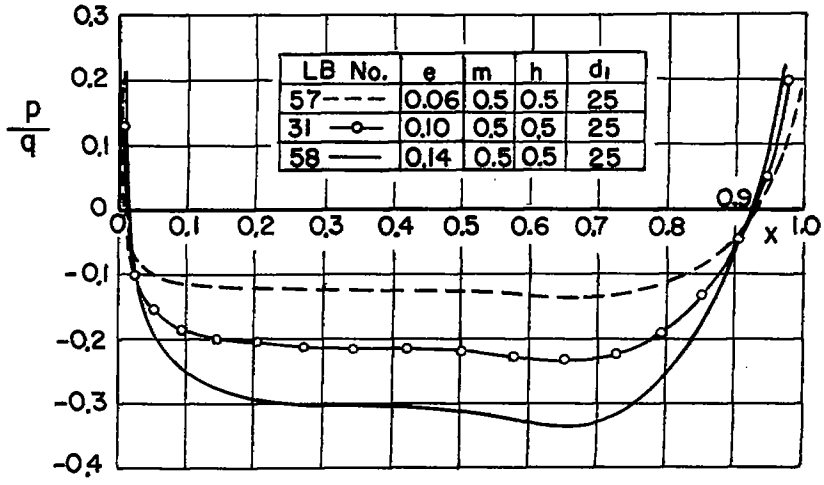

Figure 4

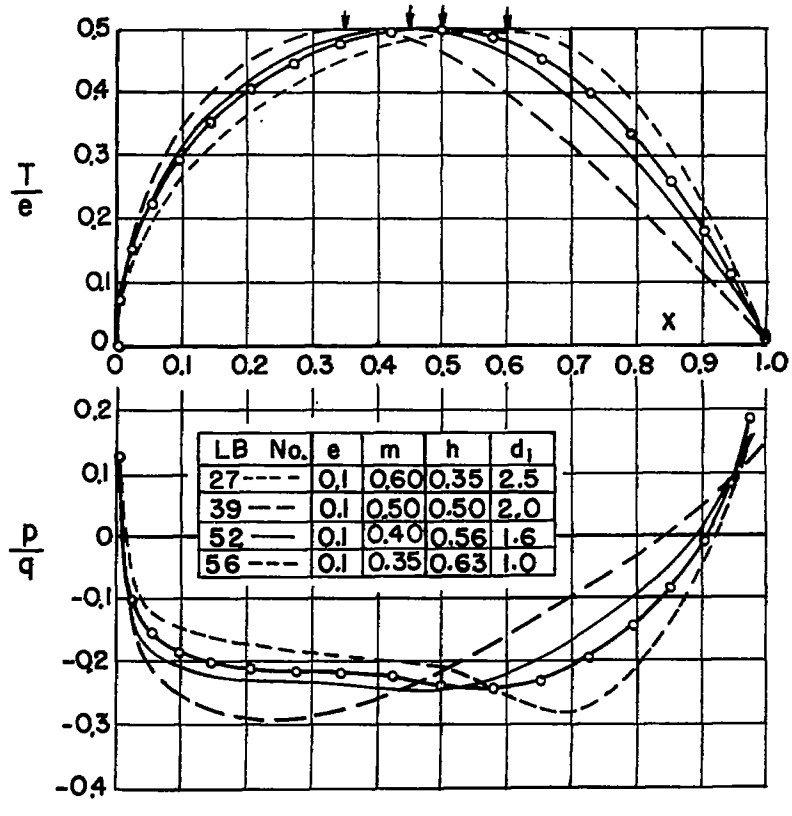

Figure 5

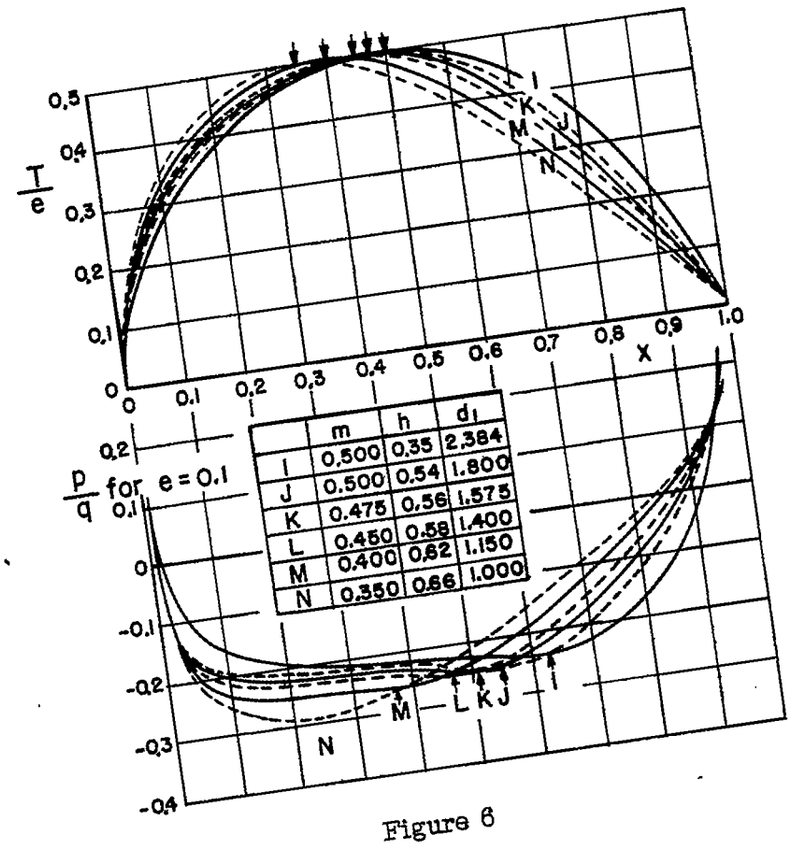

	m	h	d_1
I	0.500	0.35	2.384
J	0.500	0.54	1.800
K	0.475	0.56	1.575
L	0.450	0.58	1.400
M	0.400	0.62	1.150
N	0.350	0.66	1.000

Figure 6

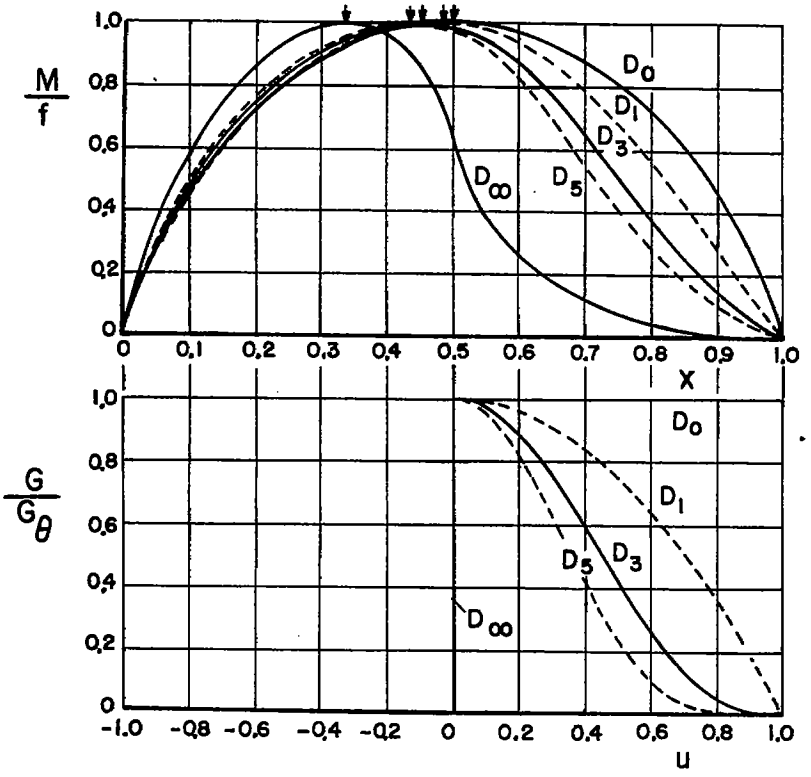
M/f
1.0
0.8
0.6
0.4
0.2
0
0 0.1 0.2 0.3 0.4 0.5 0.6 0.7 0.8 0.9 1.0
X
D0
D1
D3
D5
D∞
G/Gθ
1.0
0.8
0.6
0.4
0.2
0
-1.0 -0.8 -0.6 -0.4 -0.2 0 0.2 0.4 0.6 0.8 1.0
u
D0
D1
D5
D3
D∞

Figure 7

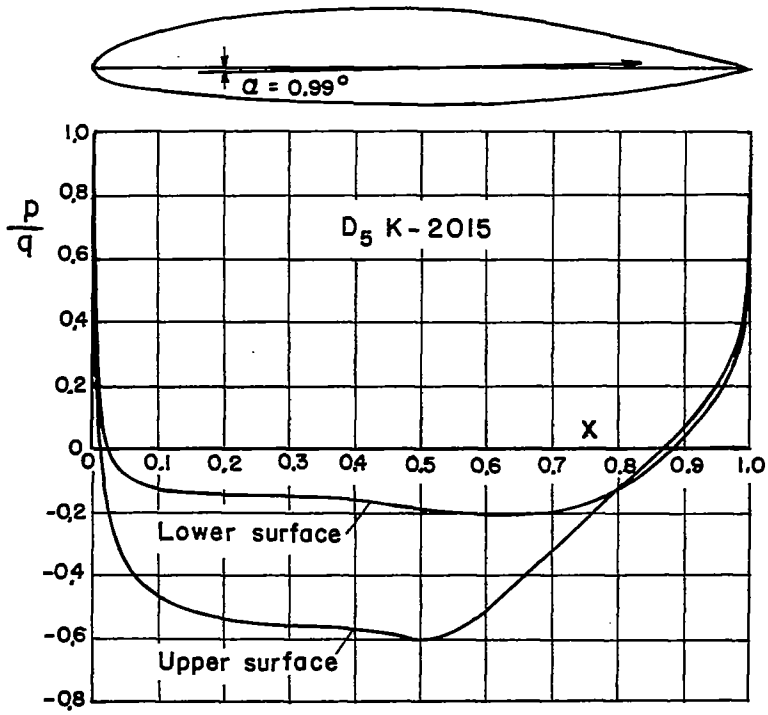
α = 0.99°
p/q
D5 K-2015
X
1.0
0.8
0.6
0.4
0.2
0
-0.2
-0.4
-0.6
-0.8
0
0.1
0.2
0.3
0.4
0.5
0.6
0.7
0.8
0.9
1.0
Lower surface
Upper surface

Figure 8

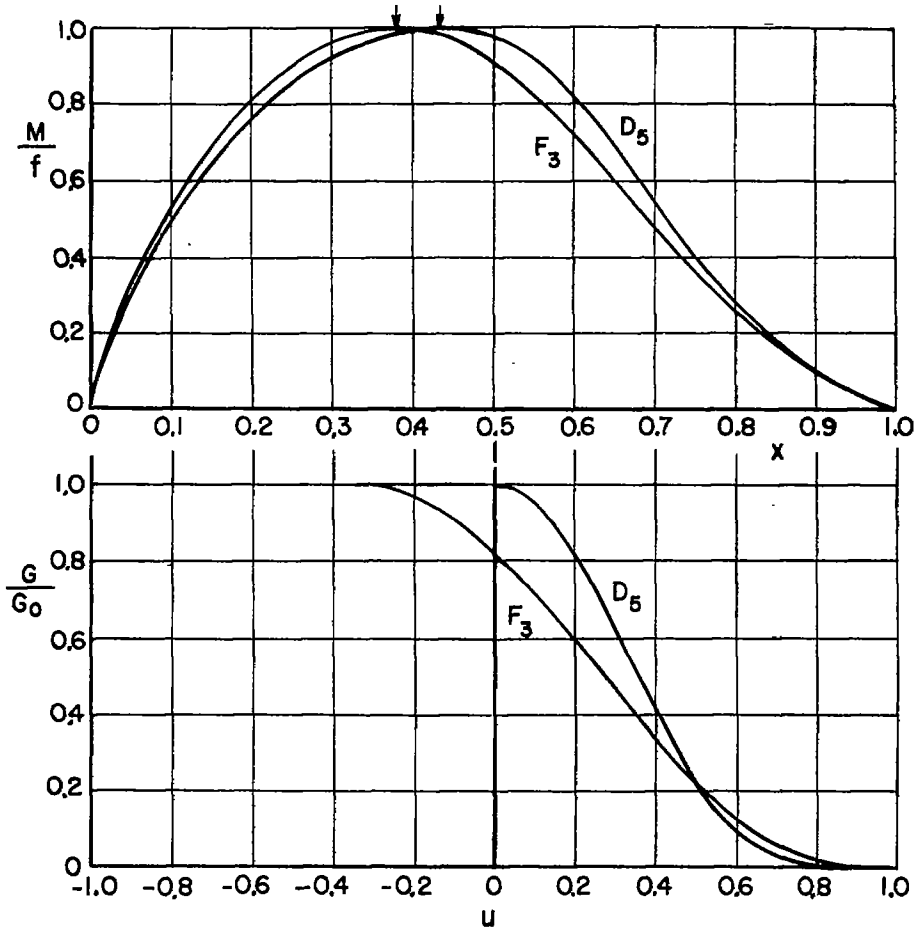
M/f
1.0
0.8
0.6
0.4
0.2
0
0
0.1
0.2
0.3
0.4
0.5
0.6
0.7
0.8
0.9
1.0
x
D5
F3
G/G0
1.0
0.8
0.6
0.4
0.2
0
-1.0
-0.8
-0.6
-0.4
-0.2
0
0.2
0.4
0.6
0.8
1.0
u
D5
F3

Figure 9

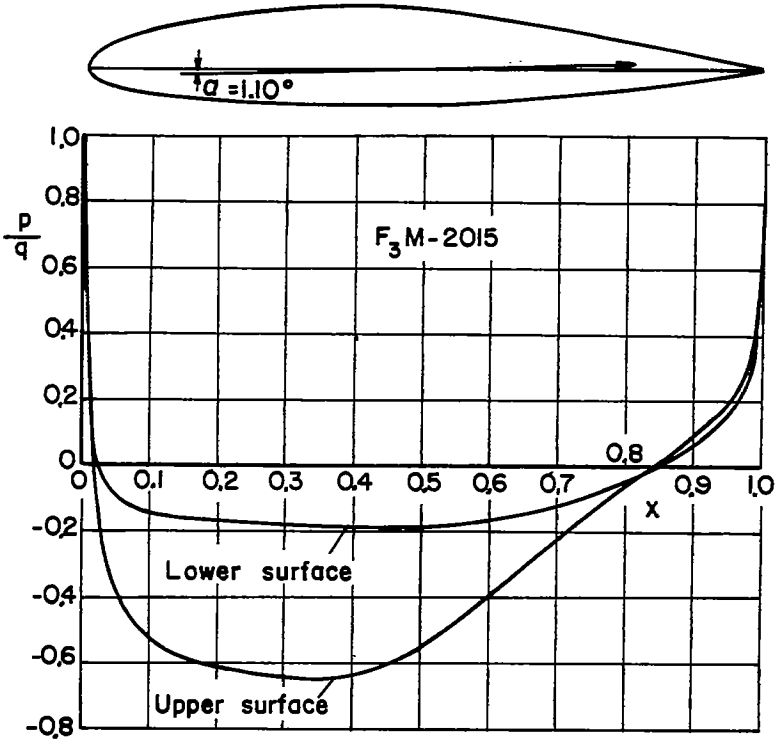

Figure 10

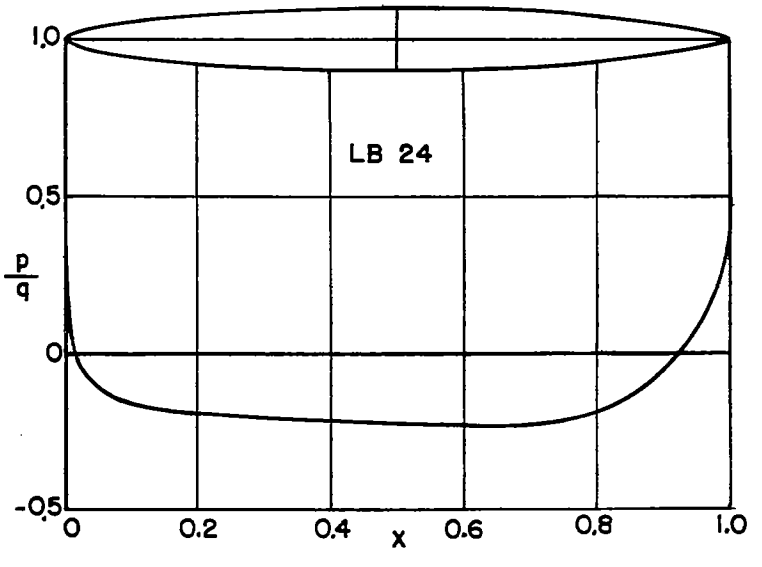

Figure 11

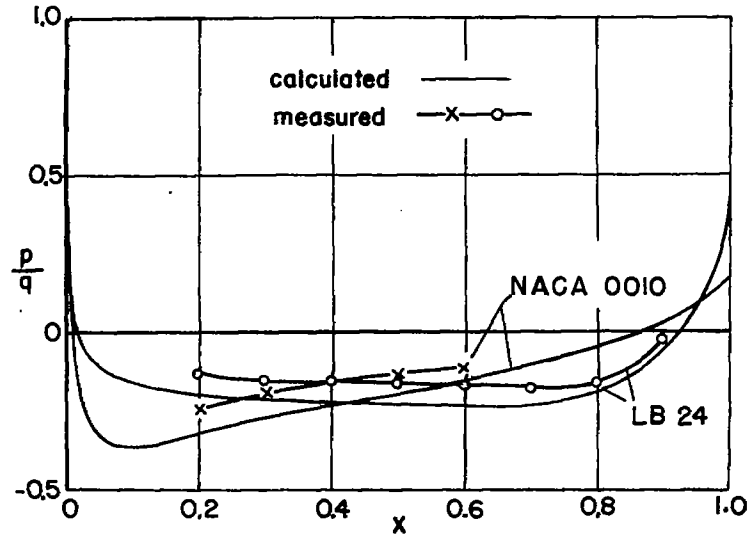

Figure 12

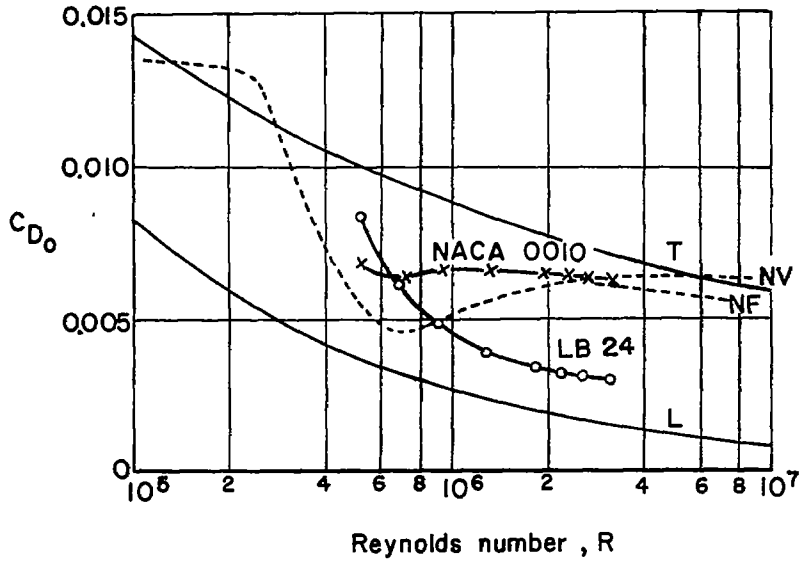

Figure 13

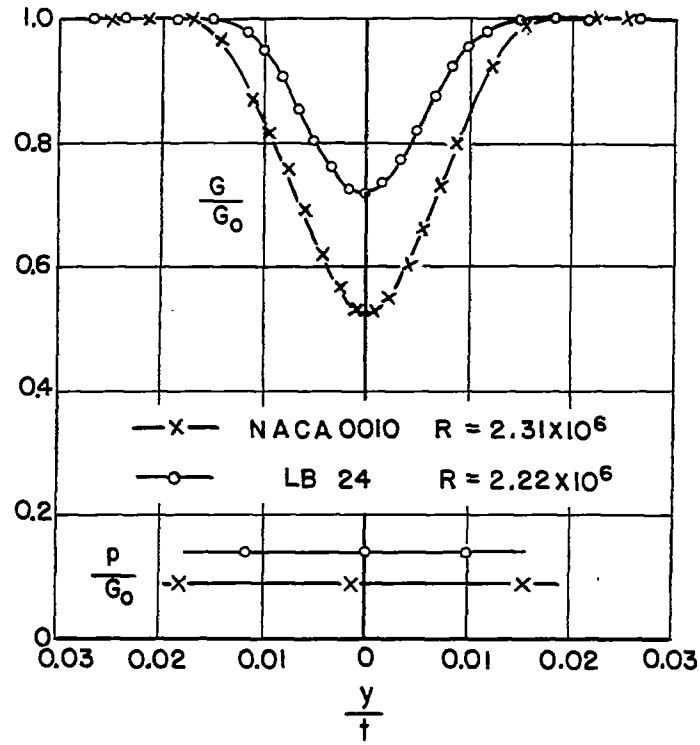

Figure 14

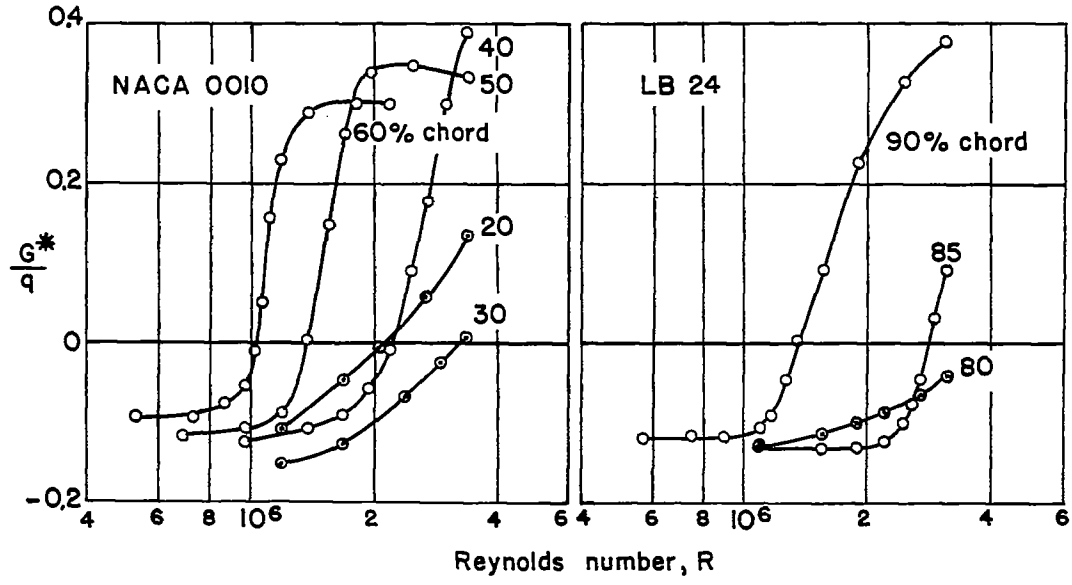

Figure 15

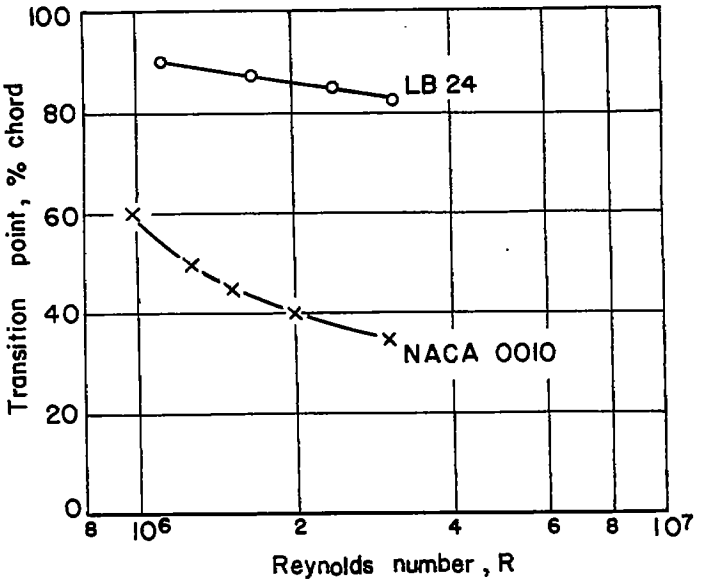

Figure 16

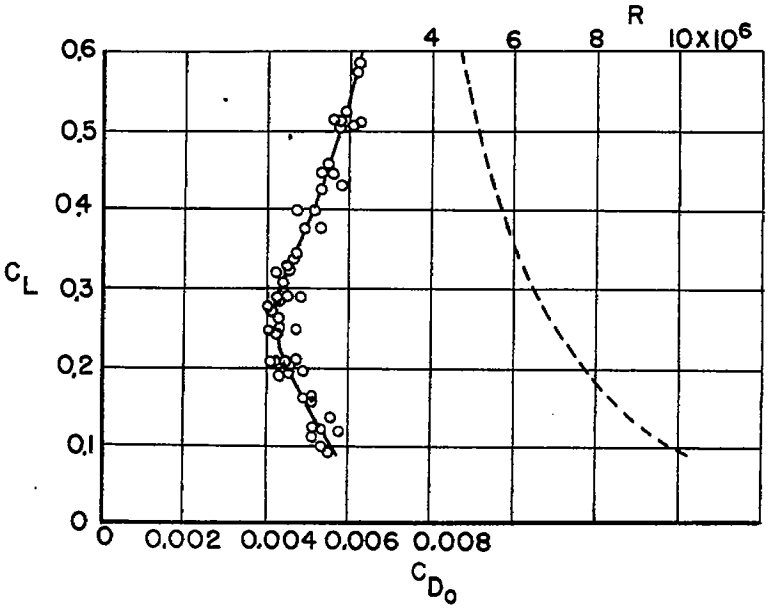

Figure 17

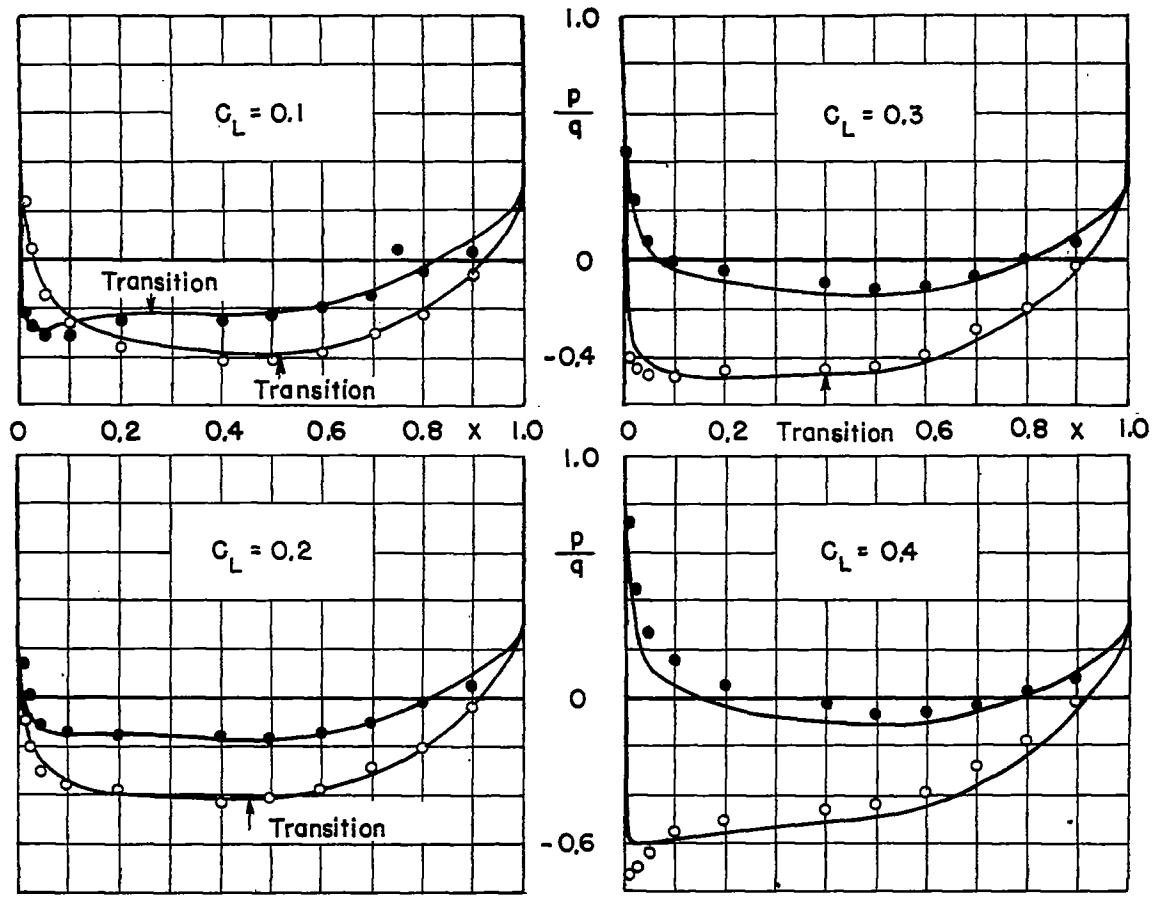
C_L = 0.1
Transition
Transition
C_L = 0.3
Transition
C_L = 0.2
Transition
C_L = 0.4
1.0
p/q
0
-0.4
-0.6
0
0.2
0.4
0.6
0.8
x
1.0
Measured o ● (o upper surface ● lower surface)
Calculated

Figure 18

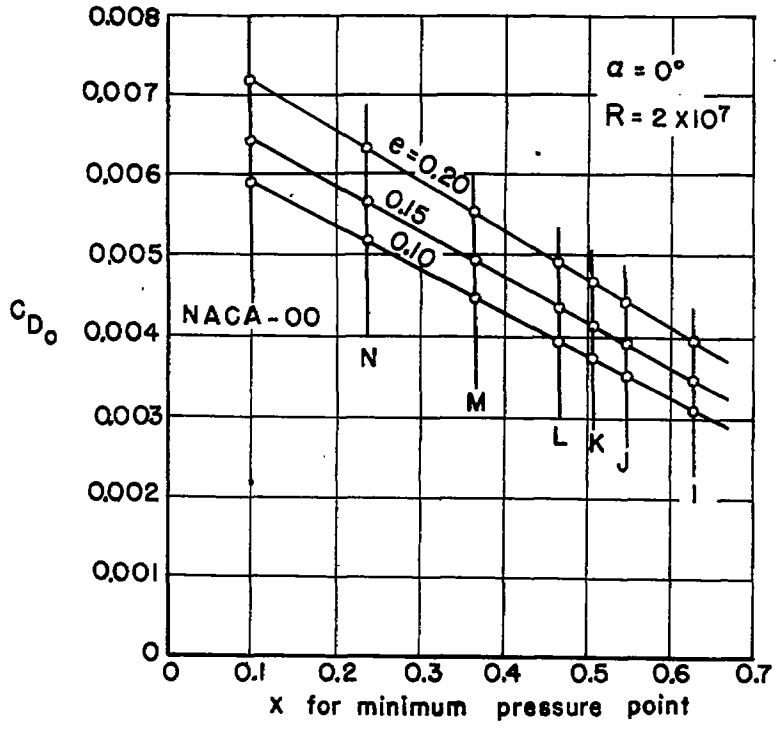

Figure 19

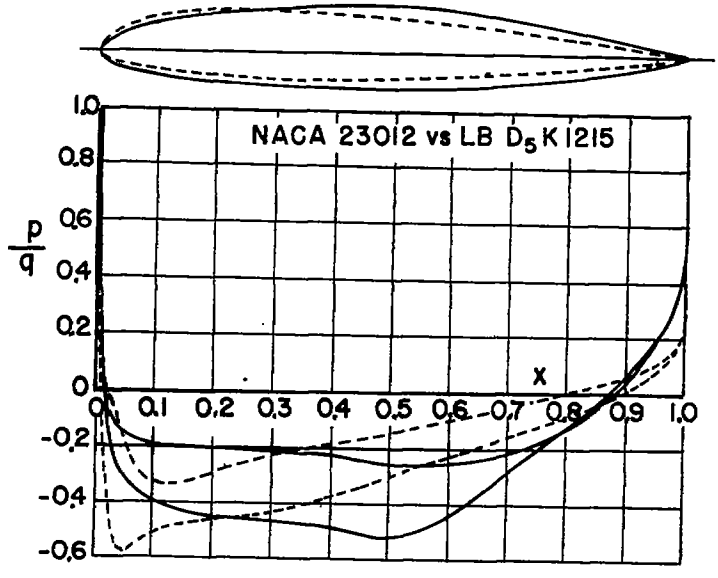

Figure 20

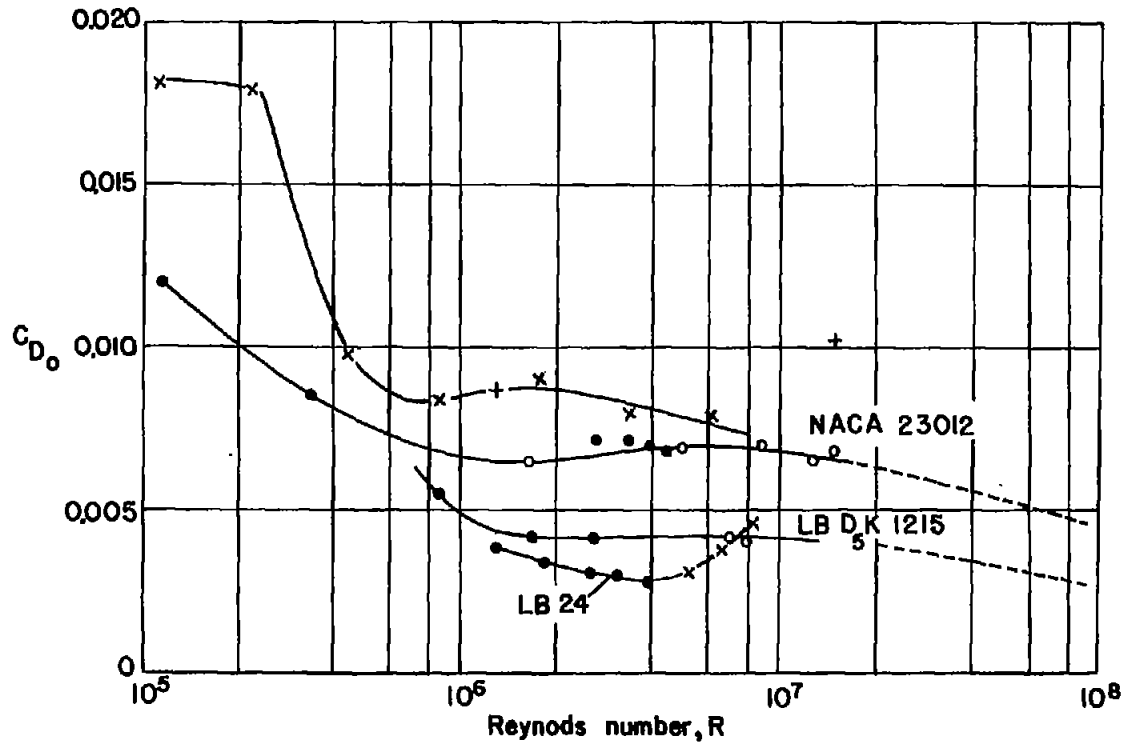
0.020
0.015
0.010
0.005
0
C_{D_o}
10^5
10^6
10^7
10^8
Reynods number, R
NACA 23012
LB D_5K 1215
LB 24

Figure 21

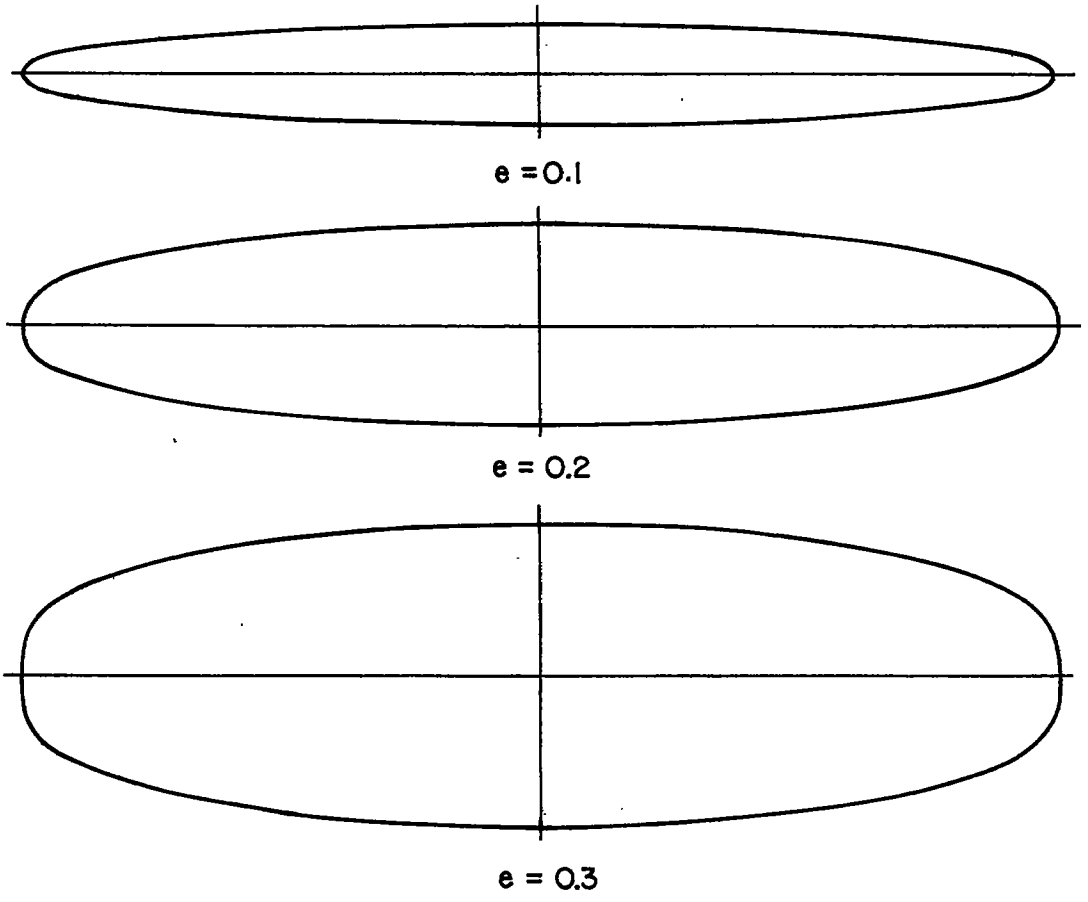

Figure 22

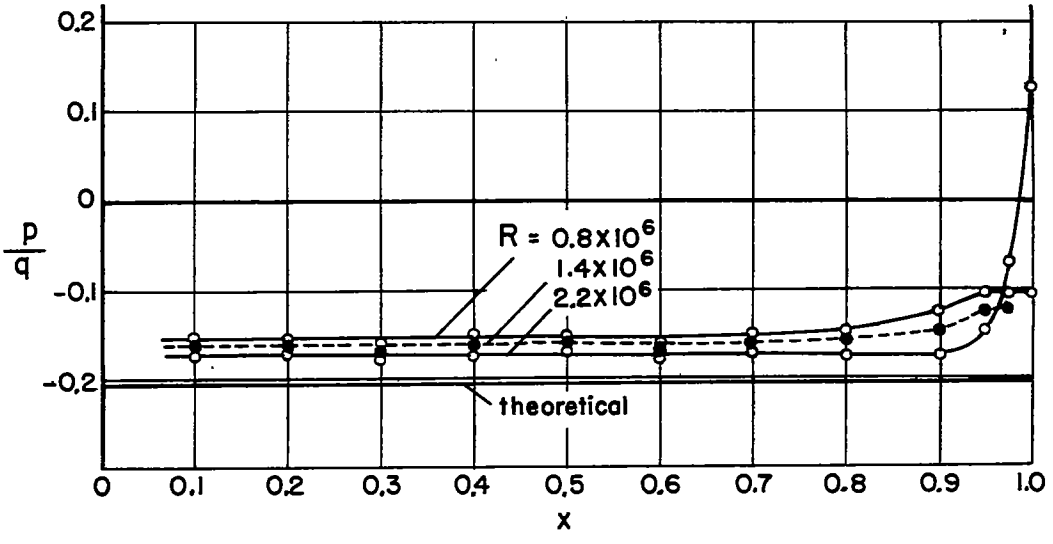
0.2
0.1
0
-0.1
-0.2
p/q
R = 0.8x10^6
1.4x10^6
2.2x10^6
theoretical
0
0.1
0.2
0.3
0.4
0.5
0.6
0.7
0.8
0.9
1.0
x

Figure 23

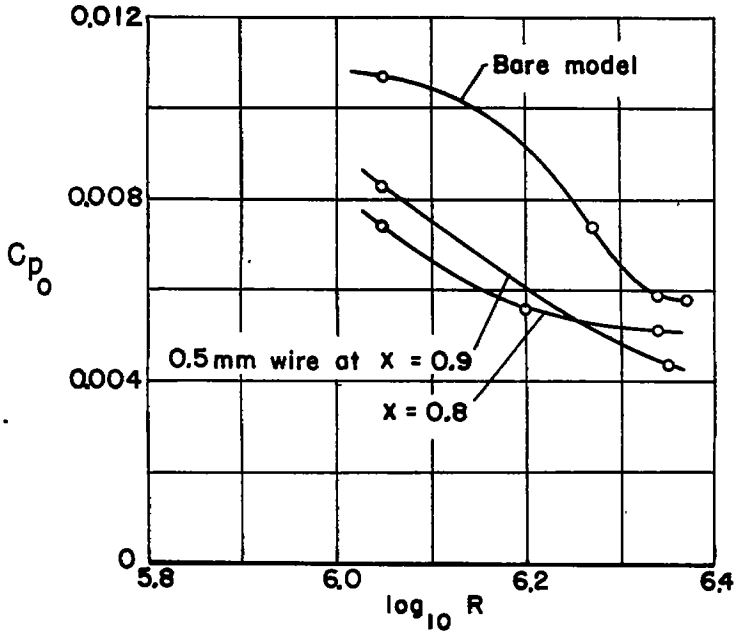

Figure 24

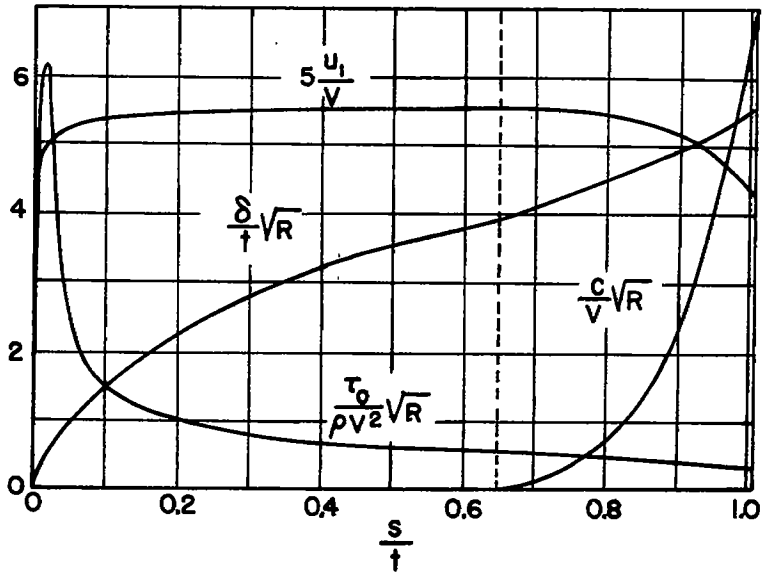

Figure 25

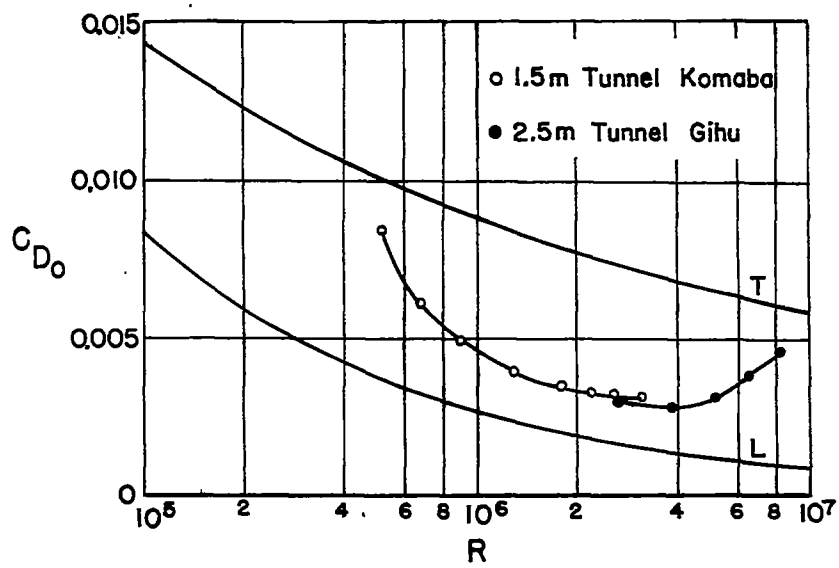

Figure 26

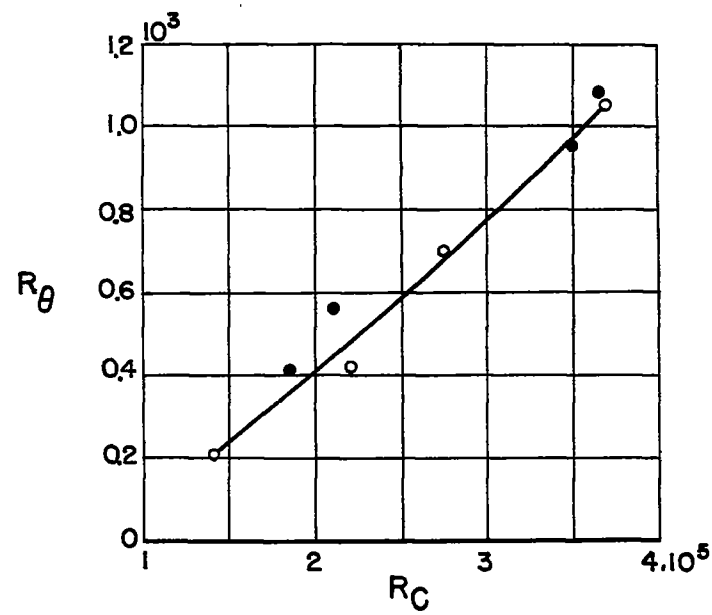

Figure 27

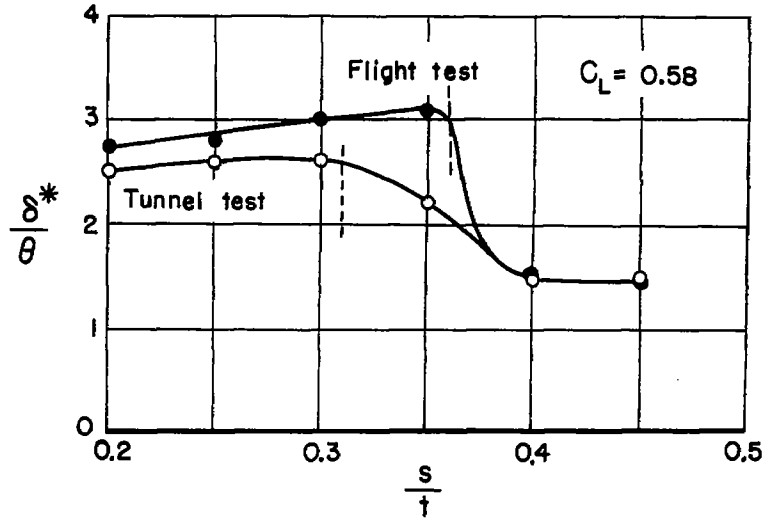

Figure 28

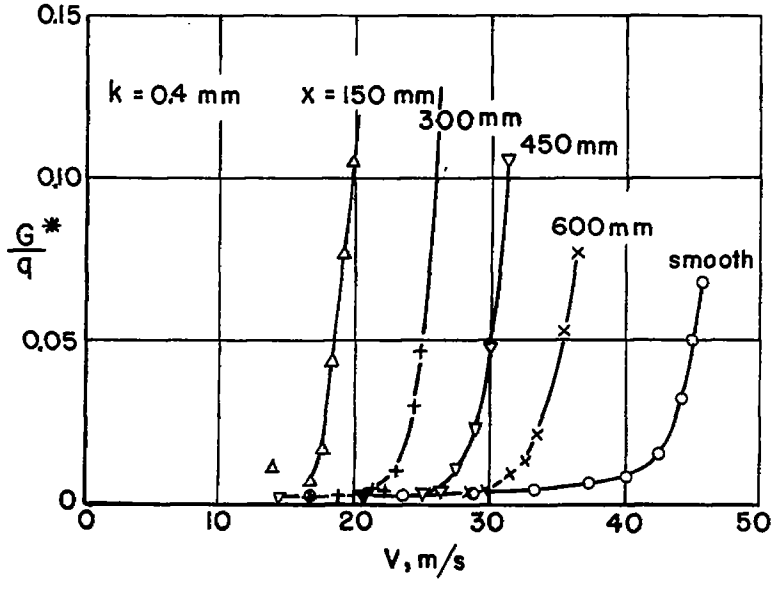

Figure 29

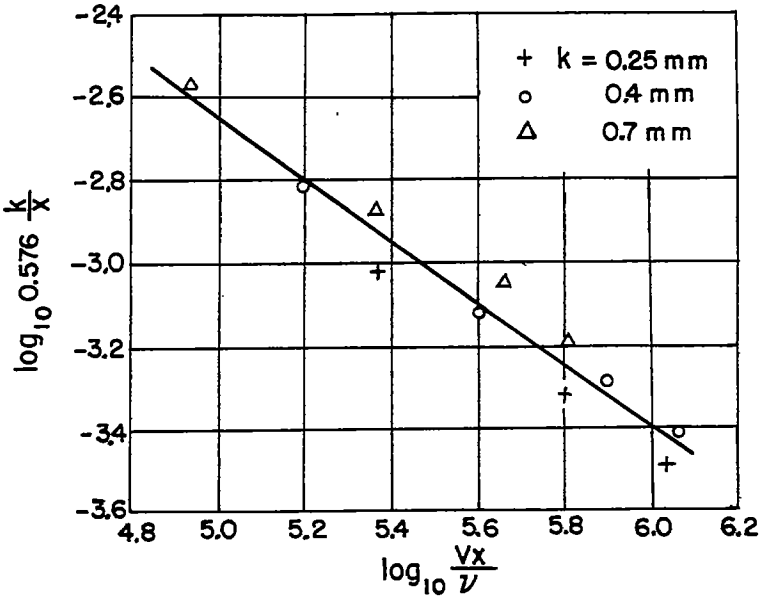

Figure 30

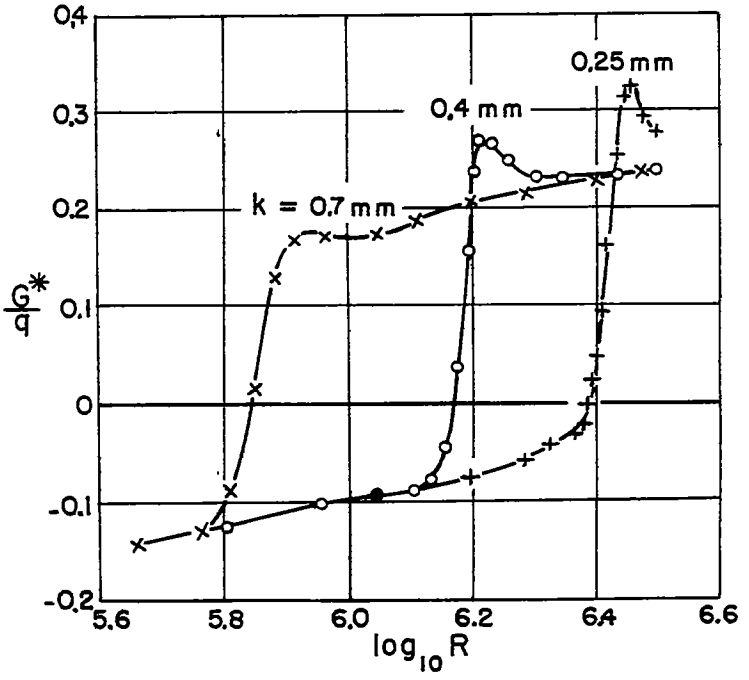

Figure 31

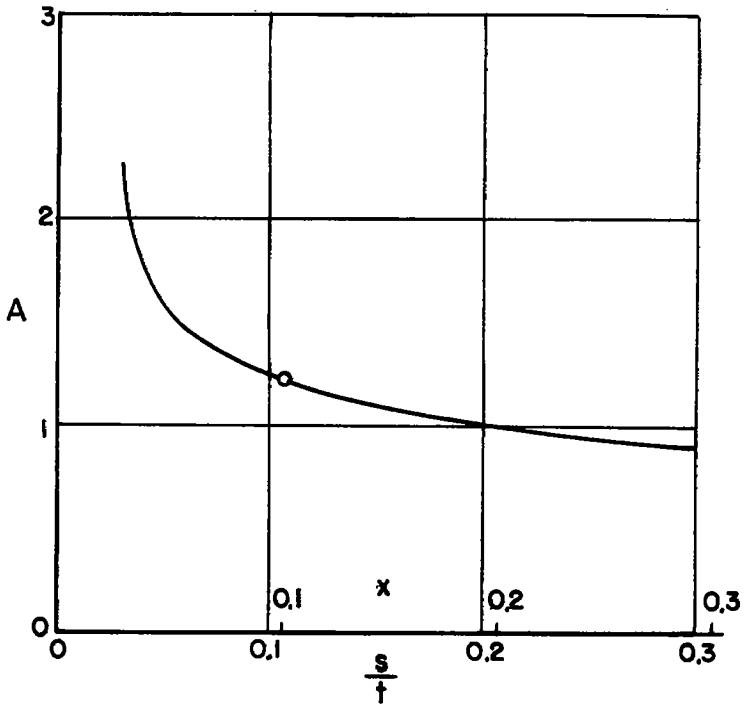

Figure 32

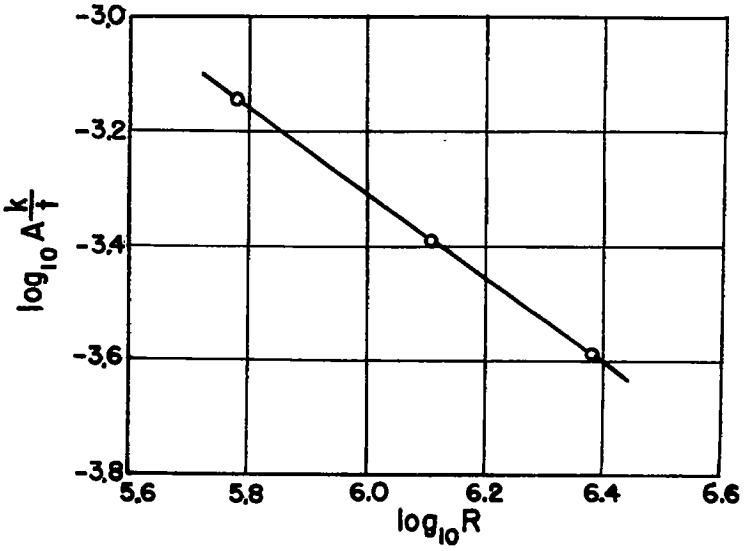

Figure 33

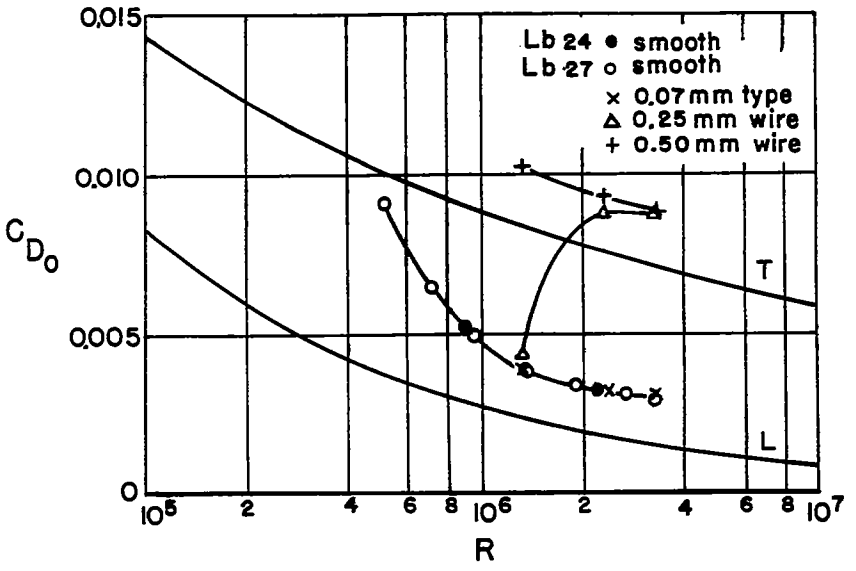

Figure 34

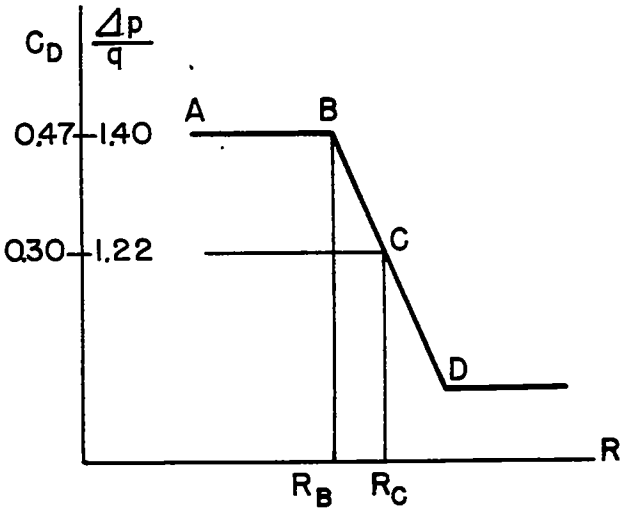

Figure 35

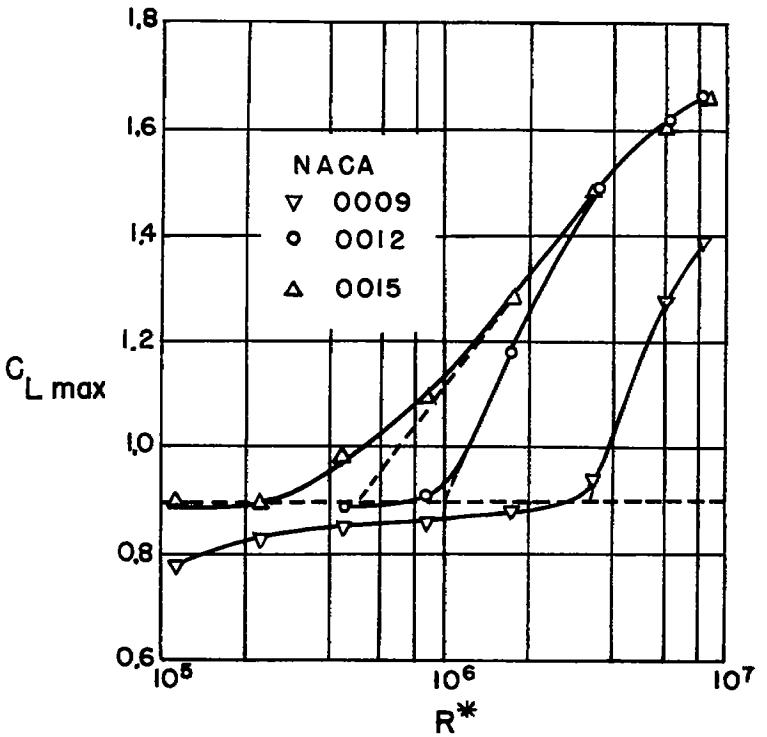

Figure 36

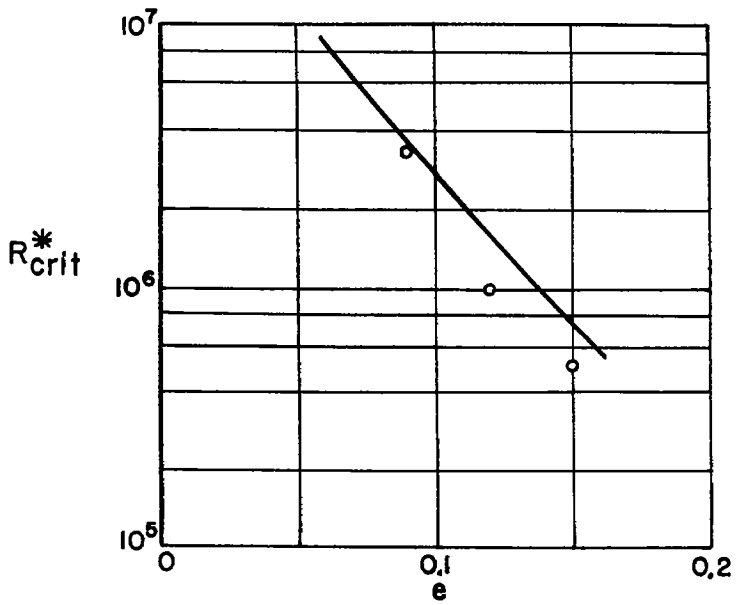

Figure 37

NACA-Langley - 10-24-52 - 1000